EPSC2017

TP2 abstracts

EPSC Abstracts
Vol. 11, EPSC2017-60, 2017
European Planetary Science Congress 2017

Spectroscopy of sulfides in the simulated environment of Mercury and their detection from the orbit

I. Varatharajan (1), A. Maturilli (1), J. Helbert (1), H. Hiesinger (2)
(1) Institute for Planetary Research, German Aerospace Center DLR, Berlin, Germany, (2) Wilhelms Universität Münster, Germany

1. Introduction

Understanding the distribution and abundance of volatiles in the planet's surface helps to understand the thermal evolution of planet itself. Mercury Surface, Space Environment, Geochemistry, and Ranging (MESSENGER) revealed that Mercury (unlike Moon) has been formed at highly reducing environment with high magnesium and surprisingly sulfur abundances [1]. Sulfide minerals are strongly proposed to be identified in Mercury in regolith. Sulfides in the shallow regolith probably include major FeS and CaS [2]. MESSENGER also suggests the presence of MnS, FeS, CrS, and TiS on the surface [3]. The sulfides are also positively detected in the Dominici crater using MESSENGER Mercury Atmospheric and Surface Composition Spectrometer (MASCS) datasets [4].

In order to detect the mineral diversity of these sulfides, it is essential to study the spectral variations along broad wavelength range in their respective simulated laboratory conditions. The spectral reflectance of sulfides which are thermally processed under Mercury conditions for the wide spectral range (0.2-100 µm) was mostly missing so far. In this study, we report the measured reflectance of a large set of sulfides in 0.2-100 µm at various phase angles. This supports the analysis of measurements from past (MASCS on MESSENGER at phase angle > 80°) and future missions (visible–near-infrared imaging spectrometer (VIHI) of Spectrometer and Imagers for MPO BepiColombo – Integrated Observatory SYStem (SIMBIO-SYS) on BepiColombo at phase angle < 30°) (Fig. 1).

2. Samples

The synthetic powdered sulfides used in the study includes MgS, FeS, CaS, CrS, TiS, NaS, and MnS. They have typically grain size of about ~10 µm. Our measurements are carried out on these synthetic samples of at least 99% purity procured from certified industrial suppliers.

3. PSL

Two Bruker Vertex 80V instruments hosted at Planetary Spectroscopy Laboratory (PSL) at the Institute of Planetary Research (PF) at the German Aerospace Center (DLR), Berlin are used for the emissivity and reflectance measurements. One of these instruments is attached to an external emissivity chamber for direct emissivity measurements at very high temperatures. One of the spectrometers is optimised for spectral measurements in the ultraviolet (UV: 0.2-0.6 µm), visible-infrared (VIS-IR: 0.4-1 µm) range, the second for the mid infrared (MIR: 1-25 µm), and Far infrared (FIR: 14-100 µm). Their corresponding specifications are tabulated in Table 1.

Table 1: Detector and Beamsplitters used for Reflectance measurements

Spectra	Detector	Beam-splitter
UV	GaP	CaF_2
VIS/IR	Si diode	CaF_2
MIR	MCT	KBr Broadband
FIR	DTGS201	Mylar

4. Methods

In the study, we thermally processed the fresh synthetic sulfides by heating them slowly up to 500ºC in vacuum and during the process, we measured the thermal radiance/emissivity of these sulfides in the thermal infrared spectral region (TIR: ~7-14 µm) at the interval of every 100ºC [5, 6]. After this, we collectively measured the spectral reflectance at vacuum of fresh and heated synthetic sulfides at wide spectral range (0.2-100 µm) at four different phase angles, 26º, 40º, 60º, 80º.

5. Results

As reported before [6] the emissivity is measured at thermal range of 7-14 µm at temperatures of 100-500 °C which will support the Mercury Radiometer and Thermal Imaging Spectrometer (MERTIS) payload of BepiColombo mission.

The thermally processed samples are then used to measure the spectral reflectance at wide spectral range of 0.2-100 µm at four phase angle measurements. The spectral profile for Phase 80° (Fig. 1a) will further help us to identification of sulfides in available MESSENGER MASCS datasets. In the UVVIS spectral range (0.3-0.6 µm), both fresh and heated sulfides of CaS, NaS, and MgS show stronger absorption near 0.3 µm at UV wavelength. MnS show distinctive spectral bands at 0.52 µm. All the fresh and heated sulfides both show minor and sharp bands near 0.22 and 0.26 µm. These spectral features did not change with respect to phase angle and temperature.

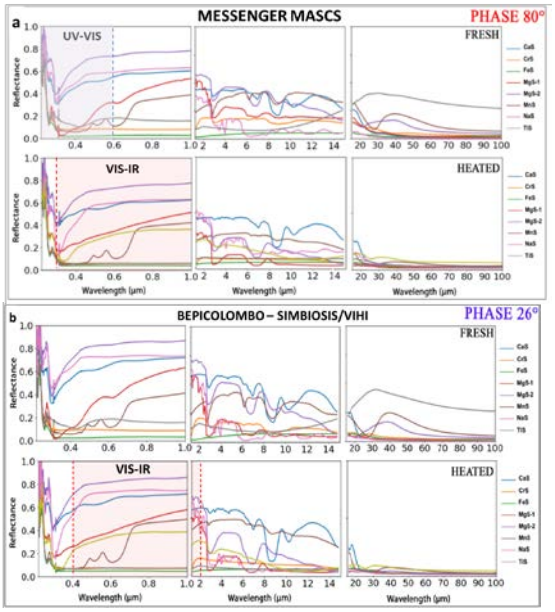

Figure 1: a) The spectral measurements supporting the detection of fresh and heated sulfides in available MESSENGER MASCS; b) The spectral reflectance measurements of fresh and heated sulfides supporting their detection by BepiColombo-Simbio-sys/VIHI.

The thermal weathering of sulfides did not influence their spectral nature in the ultraviolet. In the laboratory reflectance spectra of fresh and heated sulfides in the MASCS VIRS spectral channel (0.3-1.45 µm) spectral channel do not show any distinctive bands except for MnS which shows strong spectral absorption features near 0.52 and 0.6 µm. However most of the sulfides have a steeper slope gradient at 0.3-0.4 µm with minor absorption near 1.1 µm (Fig.1). It is important to understand the spectral behavior of these sulfides as a function of phase angle and temperature effects. Fig. 1(a,b) shows that sulfide spectra are immune to phase angle effects with decrease in spectral range of measurement. UVVIS (0.3-0.6 µm) show no spectral variations in accordance with the change in phase angle, however, the absorption strength and albedo of the spectra is slightly diminished with increased phase angle observation in the spectral range > 1 µm. Also, the reflectance spectra of heated sulfides in FIR spectral range (15-100 µm) show an almost complete loss of the spectral features of their fresh counterparts. In order to understand the behavior of the spectral features of sulfides with respect to temperature, further extended studies are ongoing. The future work will concentrate on prolonged heating of sulfides in Mercury environmental conditions and their step-by-step change in spectral behavior along with its crystallography.

References

[1] Nittler, L.R., et al.: The Major-Element Composition of Mercury's Surface from MESSENGER X-ray Spectrometry. Science, 333(6051): p. 1847-1850, 2011.

[2] Helbert, J., A. Maturilli, and M. D'Amore: Visible and near-infrared reflectance spectra of thermally processed synthetic sulfides as a potential analog for the hollow forming materials on Mercury. Earth and Planetary Science Letters, 369–370: p. 233-238, 2013.

[3] E. Vander Kaaden, K., et al.: Geochemistry, mineralogy, and petrology of boninitic and komatiitic rocks on the mercurian surface: Insights into the mercurian mantle. Icarus, 285: p. 155-168, 2017.

[4] Vilas, F., et al.: Mineralogical indicators of Mercury's hollows composition in MESSENGER color observations. Geophysical Research Letters, 43(4): p. 1450-1456, 2016.

[5] Maturilli, A., et al.: Emissivity Spectra of Analogue Materials at Mercury P-T Conditions, in 48th Lunar and Planetary Science Conference, p. 1427, 2017.

[6] Varatharajan, I., et al.: Thermal infrared spectroscopy of Mg-sulfides at simulated Mercury's surface conditions. 48th Lunar and Planetary Science Conference, p. 1398, 2017.

EPSC Abstracts
Vol. 11, EPSC2017-188-2, 2017
European Planetary Science Congress 2017

Spectral clustering reveals similar behavior between Mercury's hollows

A. Lucchetti (1), M. Pajola (2,3,1), C. Carli (4), V. Galluzzi (4), G. Cremonese (1), L. Giacomini (4), G. A. Marzo (5) and T. Roush (3)

(1)INAF-Astronomical Observatory of Padova, 35131 Padova, Italy (alice.lucchetti@oapd.inaf.it); (2) Universities Space Research Association, NASA NPP Program (Supported by an appointment at NASA Ames Research Center: maurizio.pajola@nasa.gov); (3) NASA Ames Research Center, Moffett Field, CA 94035, USA; (4) INAF-IAPS Roma, Istituto di Astrofisica e Planetologia Spaziali di Roma, Italy; (5) ENEA Centro Ricerche Casaccia, 00123 Rome, Italy.

Introduction

The Mercury Dual Imaging System (MDIS, [1]) onboard NASA MESSENGER (MErcury Surface, Space ENvironment, GEochemistry, and Ranging) spacecraft, provided high-resolution images of Mercury surface showing that specific areas exhibiting high reflectance and relative bluer colors were composed of shallow, irregular and rimless, flat-floored depressions with bright interiors and halos, often found on crater walls, rims, floors and central peaks [2,3,4]. These features were named "hollows": they are fresh in appearance and may be actively forming today via a mechanism that involves depletion of subsurface volatiles [2,5]. Understanding the composition of these features provides additional information on Mercury's surface characterization. Therefore, we decide to perform a spectral clustering on different hollows located on the surface of Mercury. The approach was previously applied to the Dominici crater's hollows bringing successful results [6]. In this work we use the same technique to characterize other hollows cases and, specifically we study an unnamed crater located in the south-eastern corner of the Victoria quadrangle (Fig. 1).

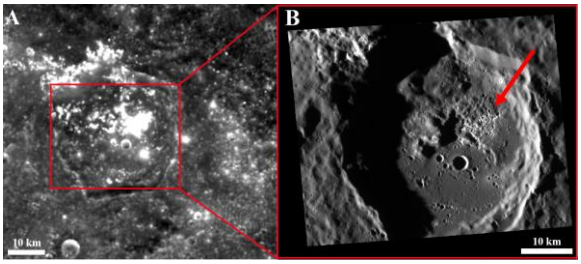

Figure 1: A: the WAC image (EW1017269227D) showing the crater under study (center latitude = 25.62°N, center longitude = -3.4°W). B: the NAC image (EN1022224039M) showing hollows in the center of the crater (red arrow).

1. Method

The MDIS imager was equipped with a monochromatic narrow angle camera (NAC), and a multiband wide angle camera (WAC), used to investigate the surface composition. Here we used the WAC dataset covering the unnamed crater with a scale of 260 m/pixel through eleven filters, ranging from 0.433 to 1.012 μm.

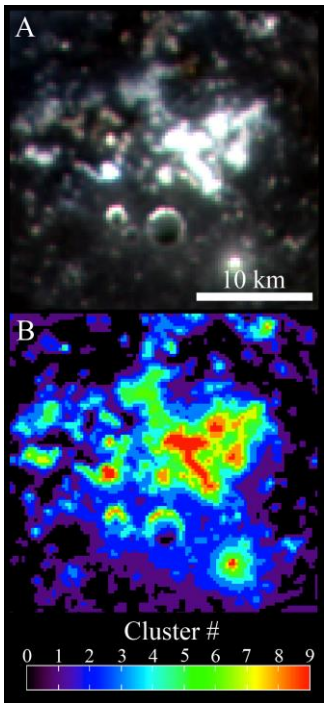

Figure 2: Above it is shown close up of the WAC reference image showing hollows (EW1017269227D), while below are reported the 10 clusters identified on the MDIS dataset.

The images have been photometrically corrected with Hapke methods [7], using the parameters derived in [8], i.e. incidence angle of 30°, emission angle of 0° and phase angle of 30°. On the photometrically corrected dataset we applied a statistical clustering over the entire dataset based on a K-means partitioning algorithm [9]. It was developed and

evaluated by [9-11] and makes use of the Calinski and Harabasz criterion [12] to find the intrinsically natural number of clusters, making the process unsupervised. A natural number of ten clusters was identified within the crater and its closest surrounding, see Fig. 2. Each resulting cluster is characterized by an average multi-color spectrum, and its associated variability. This approach has been previously applied for compositional interpretation of different Solar System objects, e.g. asteroids, Mars, Phobos and Iapetus [11, 13, 14, 15]. The algorithm is agnostic of the physical meaning of the resulting clusters, and scientific interpretation is required for their subsequent evaluation.

2. Results and Future works

The application of the spectral clustering technique provides similar results to the previously analysis regarding the Dominici crater [1]. Indeed, we found that hollows clearly present a wide absorption band between 0.558 and 0.828 μm that could be a possible diagnostic absorption indicative of sulfides (as reported in [6, 16]), and a hint of absorption towards the IR (Fig. 3). The application of the clustering technique permits to study in deeper detail the spectral differences characterizing craters hosting hollows. In particular by means of this method, we can correlate different spectral units with well-defined geomorphological ones. Therefore, the next step is to perform detailed geomorphological maps of the features under study in order to make a comparison with the spectral clustering results. In addition, we are studying other craters hosting hollows in order to find if these features exhibit similar spectral behavior all over the planet surface.

Acknowledgements

This activity has been realized under the BepiColombo ASI-INAF contract no.I/022/10/0. M. Pajola was supported for this research by an appointment to the National Aeronautics and Space Administration (NASA) Post-doctoral Program at the Ames Research Center administered by Universities Space Research Association (USRA) through a contract with NASA.

References

[1] Hawkins, S. E. et al. (2007), *Space Sci. Rev.*, 131, 247-338 [2] Blewett D. T, et al. (2011) *Science*, 333, 1856–1859. [3] Blewett D. T. et al. (2013) *JGR Planets*, 118, 1013-1032. [4] Thomas R. J. et al. (2014), *Icarus*, 229, 221–235. [5] Vaughan W. M. et al. (2012) LPSC, 43, abstract 1187. [6] Lucchetti, A. et al. (2017), LPSC. [7] Hapke, B. (2002), *Icarus*, 157, 523-534. [8] Domingue, D. et al. (2015), *Icarus*, 257, 477-488. [9] Marzo, G. et al. (2006) *JGR*, 111, E03002. [10] Marzo, G. et al. (2008), *JGR*, 113, E12009. [11] Marzo, G. et al. (2009), *JGR*, 114, E08001. [12] Calinski, T., Harabasz, J., (1974), *Commun. Statist.* 3, 1–27. [13] Pinilla-Alonso, N. et al. (2011), *Icarus*, 215, 1, 75. [14] Dalle Ore, C. et al. (2012), *Icarus*, 221, 2, 735. [15] Pajola, M. and Roush, T. (2016), American Astronomical Society, DPS meeting #48, id.428.05. [16] Vilas, F. et al. (2016), *GRL*, 43, 1450-1456.

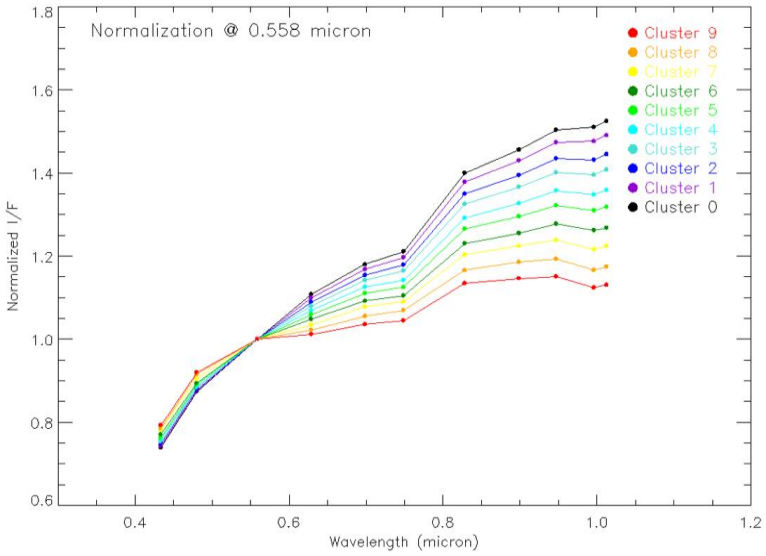

Figure 3: The average normalized spectra derived on all the identified clusters. Colors refers to Fig. 2. The legenda shows the cluster # and its not normalized I/F value at 0.558 μm

EPSC Abstracts
Vol. 11, EPSC2017-283, 2017
European Planetary Science Congress 2017

Colour mapping of the Shakespeare (H-03) quadrangle of Mercury

N. Bott (1), A. Doressoundiram (1), D. Perna (1), F. Zambon (2), C. Carli (2) and F. Capaccioni (2)
(1) LESIA - Observatoire de Paris - CNRS - UPMC - Université Paris-Diderot, 5 place Jules Janssen, 92195 Meudon, France,
(2) Istituto di Astrofisica e Planetologia Spaziali - INAF, Roma, Italy (nicolas.Bott@obspm.fr)

Abstract

We will present a colour mapping of the Shakespeare (H-03) quadrangle of Mercury, as well as the spectral analysis and a preliminary correlation between the spectral properties and the geological units. This work is part of an international collaboration between Italian, English and French teams, whose aim is to map Mercury's surface merging geological units and spectral units. The objectives are 1) to integrate color units with morpho-stratigraphic ones for all quadrangles and 2) to define regions of interest in support to the SIMBIO-SYS instrument onboard BepiColombo mission, contributing to its observational strategy.

1. Introduction

The Mercury Dual Imaging System (MDIS) Wide Angle Camera (WAC) onboard MESSENGER spacecraft observed Mercury with 12 different filters, ranging from 433.2 nm to 1012.6 nm. Thus, three major color units have been identified according to the slope and the reflectance of spectra [1]: high-reflectance plains, intermediate terrain, and low-reflectance material. A variation in the abundance of an opaque component depending on the unit is expected to explain this classification. Two minor color units have also been picked out: the red spots which seem to have a pyroclastic origin, and the hollows, related to impact craters.

To map Mercury, the surface has been subdivided into 15 quadrangles. Some of them have already been mapped [2,3]. The H-03 quadrangle, called “Shakespeare”, extends from 22.5° to 65° in latitude and from 180° to 270° in longitude (Figure 1).

2. Data set

Since the images from the filters at 698.8, 947.0 and 1012.6 nm are not enough to cover the quadrangle, we use data from 8 of the 11 available filters (433.2, 479.9, 558.9, 628.8, 748.7, 828.4, 898.8 and 996.2 nm) for the scientific analysis, while filter at 700 nm was used only for calibration.

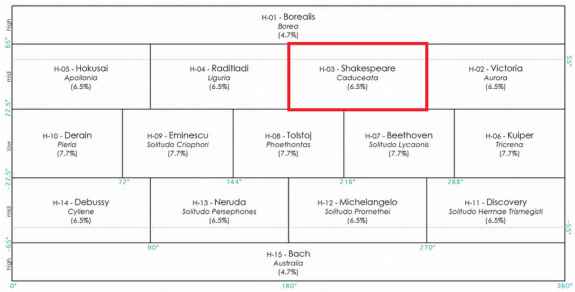

Figure 1: Location of the Shakespeare quadrangle (red rectangle) with respect to the other quadrangles

3. Method

To produce the colour map of Shakespeare, we use the software ISIS provided by USGS. We first download and import MESSENGER raw data of the quadrangle into ISIS format. We georeference the data by using the SPICE kernels for each image. We then perform a radiometric calibration to remove, for instance, the current dark and the flat field, and we project the data using an equirectangular projection. Afterwards, we apply an Hapke photometric correction – the Hapke model parameters for the combined data set [4, table 3]. The photometric correction is used to report the data at standard illumination conditions, such as those frequently used in laboratory (incidence angle i=30°, phase angle φ=30° and emission angle e=0°). Finally, we coregister the images to obtain a mosaic of Shakespeare quadrangle.

4. Results and future works

We will apply techniques of analysis, such as RGB color combinations [5,6], to emphasize differences in composition. Here we show a typical RGB map of

Shakespeare obtained with filters at 996.2, 748.7 and 433.2 nm, respectively (Figure 2). More than 50% of the quadrangle is mapped.

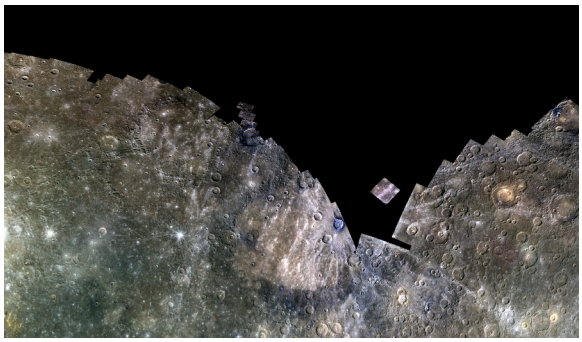

Figure 2: RGB map of the Shakespeare quadrangle (R= 996.2 nm, G=748.7 nm and 433.2 nm)

The geological map of Shakespeare is shown below (Figure 3 ; from [7]).

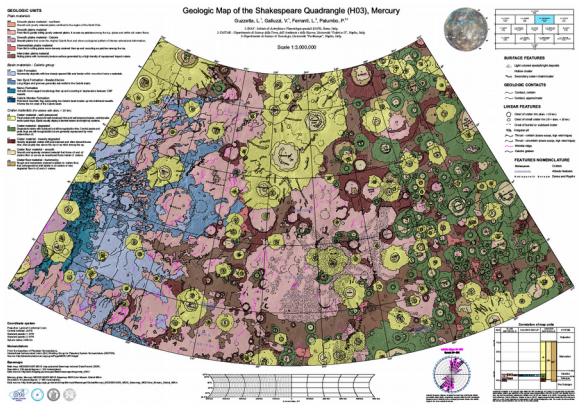

Figure 3: Geological map of the Shakespeare quadrangle

A preliminary comparison show that some color units (Figure 2) correlate to some morpho-stratigraphic ones (Figure 3), e.g. ejecta and bright deposits in Sobkou Planitia and in the cratered regions. A color contrast between West and East parts of the mapped quadrangle can be distinguished, even if this has to be confirmed by a spectral analysis. Indeed, on the RGB map (Figure 2), the East part of Shakespeare seems to be more yellow than the West part, which is consistent with a reddening of this more cratered, so older part of the quadrangle. Thus, East is likely to be more mature, i.e. more degraded by space weathering, than West. This contrast is confirmed on the geological map (Figure 3). Besides, some features like the Akutagawa and Degas craters, which appear really blue on the RGB map (Figure 2), do not show in the geological map (Figure 3) a specific unit separated from crater floor material. This higher spectral variability in specific regions will be investigated.

With the completed quadrangle, we will start to analyze in a more systematic way the spectral variability considering the combination already used in the literature (such as in [5]). Moreover, we will work on the 8 channels spectral variability looking to define some spectral units which could be associated to specific terrains and see how they can be integrated into a planetary geological map. In addition, this spectral analysis will notably help us to investigate which kind of space weathering occurs on Mercury's surface.

Acknowledgements

This work is partly supported by the Centre National d'Etudes Spatiales (CNES).

References

[1] Blewett, D. T. et al.: Multispectral images of Mercury from the first MESSENGER flyby: Analysis of global and regional color trends, Earth and Planetary Science Letters, Vol. 285, pp. 272-282, 2009.

[2] Galluzzi, V. et al.: Geology of the Victoria quadrangle (H02), Mercury, Journal of Maps, Vol. 12, pp. 227-238, 2016.

[3] Zambon, F. et al.: Mercury compositional units inferred by MDIS. A comparison with the geology in support to the BepiColombo mission, Geophysical Research Abstracts, Vol. 18, EGU2016-16909, 2016.

[4] Domingue, D. L. et al.: Mercury's global color mosaic: An update from MESSENGER's orbital observations, Icarus, Vol. 257, pp. 477-488, 2015.

[5] Denevi, B. W. et al.: The Evolution of Mercury's Crust: A Global Perspective from MESSENGER, Science, Vol. 324, pp. 613-618, 2009.

[6] Kerber, L. et al.: The global distribution of pyroclastic deposits on Mercury: The view from MESSENGER flybys 1–3, Planetary and Space Science, Vol. 59, pp. 1895-1909, 2011.

[7] Guzzetta, L. et al.: Geology of the Shakespeare quadrangle (H03), Mercury, Journal of Maps, Vol. 13, pp. 227-238, 2017.

EPSC Abstracts
Vol. 11, EPSC2017-301, 2017
European Planetary Science Congress 2017

A Dynamic Model of Mercury's Magnetospheric Magnetic Field

H. Korth (1), C. L. Johnson (2,3), L. C. Philpott (2), N. A. Tsyganenko (4), B. J. Anderson (1)
(1) The Johns Hopkins University Applied Physics Laboratory, Laurel, Maryland, USA, (2) Department of Earth, Ocean and Atmospheric Sciences, University of British Columbia, Vancouver, British Columbia, Canada, (3) Planetary Science Institute, Tucson, Arizona, USA, (4) Institute and Faculty of Physics, Saint Petersburg State University, Saint Petersburg, Russia.

1. Introduction

Mercury's solar wind and interplanetary magnetic field environment is highly dynamic, and variations in these external conditions directly control the current systems and magnetic fields inside the planetary magnetosphere. We update our static KT14 model of Mercury's magnetic field [1] by incorporating variations in the magnetospheric current systems, parameterized as functions of Mercury's heliocentric distance and magnetic activity [2] to yield the first dynamic model of Mercury's magnetospheric magnetic field. The new model, termed KT17, uses the same structure and mathematical framework as the KT14 model, but includes variable parameterizations for the magnetopause standoff distance and for the magnetotail current intensity.

2. Dependence of Parameters on Magnetic Activity

The solar wind dynamic pressure balances the magnetic pressure of the planetary field at the magnetopause so that temporal variations in ram pressure affect the location of the sub-solar magnetopause, R_{SS}. To determine the dependence of R_{SS} on magnetic activity, we followed the approach in [3]. First, we fit a model magnetopause to the magnetopause crossing locations observed during the period from Mercury orbit insertion on 24 March 2011 to the end of the MESSENGER mission on 30 April 2015. Then, the R_{SS} values were then sorted into 20%-wide bins of the magnetic disturbance index, and the average R_{SS} and Mercury's average heliocentric distance of the observations, r_h, were computed for each magnetic disturbance bin. The linear fit to the r_h-normalized R_{SS} values as function of the magnetic disturbance index shows that the magnetopause standoff distance decreases with increasing magnetic activity as is expected if the increased magnetic activity is associated with higher solar wind dynamic pressure.

An increase in magnetic activity also leads to an enhancement of the electric current that flows in the central magnetotail from dawn to dusk to form the cross-tail current sheet. The cross-tail current generates an external magnetic field, which was modeled as a superposition of a disk and a sheet current [1]. To determine variations in the cross-tail current intensity with magnetic activity, 1-min averages of magnetic field observations acquired within the magnetosphere were sorted into bins of the magnetic disturbance index each again 20% wide. The data in each bin were then fit by minimizing the root-mean-square (rms) residual of the model field with respect to the MESSENGER observations to yield the current intensity parameters for each range of magnetic activity. The minimization procedure accounts for dependence of R_{SS} on r_h determined above. Linear fits to these parameters as a function of magnetic disturbance index were calculated. Higher cross-tail current intensities were obtained for higher magnetic activity. This result is consistent with the hypothesis that elevated magnetic activity leads to higher reconnection rates, stronger circulation of magnetic flux, and, ultimately, an increase in the strength of the cross-tail current.

A magnetic activity-dependent model of Mercury's magnetic field was developed by replacing the static values of the sub-solar magnetopause standoff distance and the cross-tail current intensity parameters in the KT14 model with the linear dependencies on the magnetic disturbance index identified above. The figure below shows the magnetic field configurations of the revised model, termed KT17, for magnetic disturbance indices of 95% (black line) and 5% (blue dashed line) together with the average magnetopause (red line) for the 50% activity level. The tracing of magnetic fields lines

shows a modest change in the size of the magnetosphere in response to variations in magnetic activity.

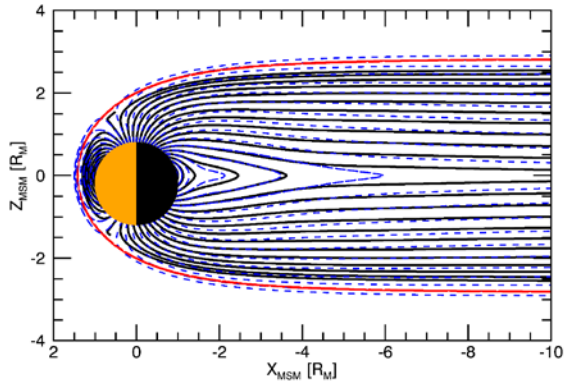

3. Summarized Discussion

The new, dynamic model reproduces the location of the magnetopause current system as a function of systematic pressure variations encountered during Mercury's eccentric orbit, as well as the increase in the cross-tail current intensity with increasing magnetic activity.

To test improvements in the model afforded by dynamic specification of parameters, we computed the residuals between the observed magnetic field and that modeled using the associated magnetic disturbance index and heliocentric distance. The rms value of these residuals is a measure for the goodness of the model, and a reduction thereof is an indicator for the improvement of the model. The rms residual of the KT17 model computed from data acquired between Mercury orbit insertion and the end of the mission is 25.3 nT and is slightly higher than the 24.8 nT reported for the KT14 model, which was fit to data acquired from orbit insertion to 28 November 2012. The increase in the magnitude of the residual field may result from higher solar activity during the later orbital mission phase as indicated by a secondary maximum in the sun spot number in 2014 that was higher than that during the first peak in 2011. Consistent with this conjecture, the rms residual of the KT14 model fit to the entire orbital dataset is 26.5 nT, which is slightly higher than the value obtained for the KT17 model. Comparison of the misfit shows that the KT17 model yields only a minor reduction of the rms residual. Thus, despite the enhancements in the external field parameterization, the residuals between the observed and modeled magnetic field inside the magnetosphere indicate that the dynamic model achieves only a modest overall improvement over the previous static model.

The spatial distribution of the residuals in the magnetic field components shows substantial improvement of the model accuracy near the dayside magnetopause. Elsewhere, the large-scale distribution of the residuals is similar to those of the static model. This result implies either that magnetic activity varies much faster than can be determined from the spacecraft's passage through the magnetosphere or that the residual fields are due to additional external current systems not represented in the model or both. Birkeland currents flowing along magnetic field lines between the magnetosphere and planetary high latitude regions have been identified as one such contribution. The remaining dependence of the magnitude of the residuals on magnetic activity is consistent with this conjecture.

Acknowledgements

The National Aeronautics and Space Administration supported this work under grant agreement NNX16AJ01G issued through the Science Mission Directorate. CLJ and LCP acknowledge support from the Natural Sciences and Engineering Research Council of Canada.

References

[1] Korth, H., N. A. Tsyganenko, C. L. Johnson, L. C. Philpott, B. J. Anderson, M. M. Al Asad, S. C. Solomon, and R. L. McNutt, Jr. (2015), Modular model for Mercury's magnetospheric magnetic field confined within the average observed magnetopause, J. Geophys. Res. Space Physics, 120, 4503–4518, doi:10.1002/2015JA021022.

[2] Anderson, B. J., C. L. Johnson, and H. Korth (2013), A magnetic disturbance index for Mercury's magnetic field derived from MESSENGER Magnetometer data, Geochem. Geophys. Geosyst., 14, 3875–3886, doi:10.1002/ggge.20242.

[3] Johnson, C. L., L. C. Philpott, B. J. Anderson, H. Korth, S. A. Hauck, D. Heyner, R. J. Phillips, R. M. Winslow, and S. C. Solomon (2016), MESSENGER observations of induced magnetic fields in Mercury's core, Geophys. Res. Lett., *43*, 2436−2444, doi:10.1002/2015GL067370.

EPSC Abstracts
Vol. 11, EPSC2017-458, 2017
European Planetary Science Congress 2017

Observational conditions for the detection of X-ray fluorescence from sodium by the MIXS instrument on BepiColumbo

R. Cooper (1), M. Grande (1), A. Martindale (2), E. Bunce (2)
(1) Aberystwyth University, UK, roc17@aber.ac.uk

(2) Leicester University, UK

Abstract

We model the expected fluorescence from the exosphere and surface of Mercury, as observed by the Mercury Imaging X-ray Spectrometer (MIXS) on the upcoming BepiColumbo mission, using code modified from that used for the SMART-1 D-CIXS instrument to the Moon. Modifications include detector parameters, solar proximity, surface elemental composition, and emission from the optically thin exosphere. From this, preferential observation parameters have been determined for MIXS during its orbit. Modelling of these observations is conducted, with particular emphasis on the sodium component.

1. Introduction

X-ray fluorescence is typically considered to be a laboratory technique, yet has been found to have numerous uses in planetary science. Due to the high solar flux at Mercury, it is considered a prime target for using this method for elemental abundance detection. The main focus of this work is the MIXS detectors on the BepiColumbo Mission, which is due to launch in October 2018. MIXS is comprised of two detectors, a collimated channel MIXS-C and a telescope MIXS-T [1]. Their primary aim is to measure surface elemental abundances; however it is feasible that MIXS will be able to answer more of the major questions about Mercury than those covered by its primary aim.

In this work, we consider the potential for MIXS to observe fluorescence from Mercury's exosphere. From this elemental abundances of the exosphere can be determined, as well as improving knowledge of surface-exosphere interaction. The main target of this fluorescence detection is the sodium component. This is due to the fact that sodium is one of the more abundant, and volatile elements present in Mercury's exosphere. To evaluate the optimal configuration of these detectors for viewing the fluorescence, a model of the fluorescence from both the surface and exosphere of Mercury has been produced.

1.1 Fluorescence model

The model used for this work was originally designed for D-C1XS on the SMART-1 mission to the Moon [2], and has been adapted for this new purpose. As the fluorescence calculations originally used will still be correct [3], they require no changes. The alterations required focus mainly on the elemental abundances, proximity to the Sun, and increased solar flux. Figure one shows the expected observations from MIXS-C when viewing the surface fluorescence from Mercury. As expected, numerous fluorescence peaks are visible, with some of the most prominent being magnesium and silicon. Sodium is not easily observed, however it isn't highly abundant on Mercury's surface so this is to be expected.

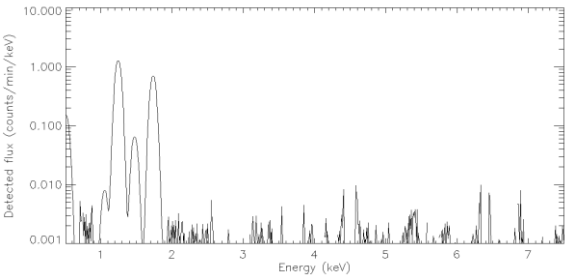

Figure 1: Model produced X-ray fluorescence spectrum for the surface of Mercury as observed by MIMXS-c for one minute during an X-class flare.

Additional model alterations are required to replicate exospheric conditions in the model. Inclusion of scale heights and an exospheric decay component produce this desired effect.

Figure two shows the fluorescence observed by MIXS when it is at a normal to the planet's surface. This therefore includes fluorescence from both the surface and exosphere combined. The sodium component is clearly visible compared to the peak in figure 1, with an expected detection rate of one photon a minute. However to obtain this result, certain conditions must be met. A high quantity of solar flux is used, along with a prolonged exposure time. Additionally, this observational configuration makes determining the exospheric fluorescence separately from the surface fluorescence impractical. This does however act as a proof of concept before more detailed observational parameters are determined.

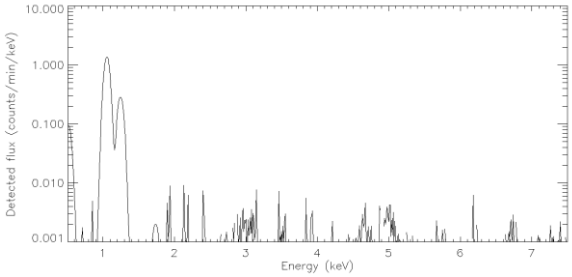

Figure 2: Model produced X-ray fluorescence if both the exosphere and surface of Mercury observed by MIXS-C for one minute during an X class solar flare.

2. Optimal observational conditions

Taking into account regions in which the detector cannot operate, it is possible to ascertain the most advantageous positions for observations. By waiting until the detector is positioned at a location shown in figure three, observations can be made through the polar region where the exospheric sodium concentration is at its most dense. This will also include the tail region of the sodium exosphere, which provides a high volume of observable sodium. It also allows for independent observation of the exospheric fluorescence, with the surface factor subtracted.

It is also necessary to consider the solar conditions required for the fluorescence to be detectable. The current launch date for BepiColumbo will place it at Mercury in a solar maximum, therefore greatly increasing the potential for such flares.

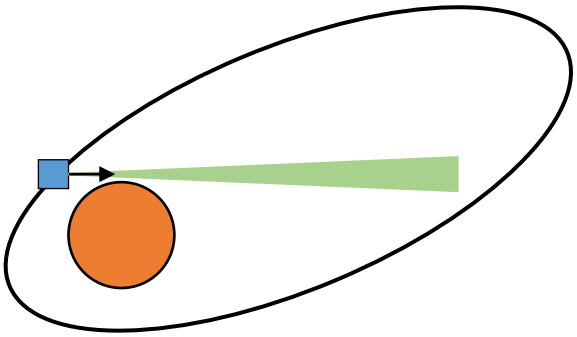

Figure 3: Optimal observational position for MIXS, modified from MPO orbital diagrams. Arrow indicates direction of observation, with additional observational cone.

3. Summary and Conclusions

The potential to observe X-ray fluorescence events at Mercury with MIXS should be capitalised on. At certain points in the proposed orbital paths around Mercury, MIXS will be in a position to observe this fluorescence, allowing for additional data for currently planned exospheric investigation. From these observations, predictions on MIXS' ability to explore the sodium tail of Mercury's exosphere will be possible, along with interactions between the exosphere and magnetosphere of the planet.

Acknowledgements

The authors would like to thank Adrian Martindale and the members of the Leicester University space research center for access to the MIXS grasp data, and the author of the original model Bruce Swinyard.

References

[1] Fraser, G. W. et al: The Mercury Imaging X-ray Spectrometer (MIXS) on BepiColumbo, Planetary and Space Science, Vol. 58, pp. 79-95, 2010

[2] Grande, M. et al: The D_CIXS X-ray mapping spectrometer on SMART-1, Planetary and Space Science, Vol. 51, pp. 427-433, 2003

[3] Clark, P. E. & Trombka, J. I.: Remote X-ray spectrometer for Near and future missions: Modeling and analyzing X-ray production from source to surface, Journal of Geophysical Research, Vol. 102, pp. 16,361-16,384, 1997

EPSC Abstracts
Vol. 11, EPSC2017-494, 2017
European Planetary Science Congress 2017

Retrieval of Mercury's h_2 from BepiColombo Laser Altimeter data

R. Thor (1, 2), R. Kallenbach (3), U. Christensen (1), and J. Oberst (2,3)
(1) Max Planck Institute for Solar System Research, Justus-von-Liebig-Weg 3, D-37077 Göttingen, (2) Technische Universität Berlin, Institute of Geodesy and Geoinformation Science, Straße des 17. Juni 135, D-10623 Berlin, (3) DLR Institute of Planetary Research, Rutherfordstraße 2, D-12489 Berlin

Abstract

We simulate the measurements which will be carried out by the BepiColombo Laser Altimeter (BELA) and investigate whether spatial resolution and temporal coverage will be sufficient to retrieve the Love number h_2. The Sun's tidal potential causes periodic radial displacements of the surface with an amplitude of $\sim$ 2 m at the equator. This displacement is measured by laser altimetry. In this study, we extract it by solving simultaneously for the static global shape of Mercury and its variability in time in a least-squares adjustment. We parametrize the shape using 2D cubic splines as basis functions. Under nominal measuring conditions, we achieve a relative accuracy of 8.7% and 2.7% after 12 and 26 months, respectively.

1 Introduction

The tidal Love number h_2 describes the vertical tidal response of the solid body and can give constraints on the interior structure of Mercury, such as inner and outer core radius and core composition [4]. Therefore, it is an important input quantity for models of the magnetic dynamo and the thermal history. So far, h_2 could not be retrieved from Mercury Laser Altimeter (MLA) data which only cover the Northern hemisphere of Mercury. The shape data to be acquired by BELA from the year 2026 on will cover much more densely both the Northern and Southern hemisphere.
The h_2 Love number of the Moon has been retrieved by comparing intersecting ground tracks [3]. As the Mercury Planetary Orbiter (MPO) will carry BELA on a near-polar orbit, intersections will be mostly very close to the poles or at sharp angles, resulting in unfavorable geometries and low amplitudes of the displacement signal. In this study, we use a different method which does not use ground track crossovers, but takes all measurements into account to solve for the static and time-variable parts of the global shape simultaneously. We use 2D cubic splines as basis functions which is an advance over previous studies which only used cubic splines in longitude direction [2] .

2 Methods

We simulate the global shape of Mercury based on low-degree spherical harmonic coefficients derived from a photogrammetric digital elevation model [1]. These simulations are necessary to assess the uncertainty induced by a specific shape realization. We also simulate the orbit of MPO using the official pre-mission trajectory models provided by ESA. Simulated measurements assume nominal instrument operation conditions and a priori values for the libration amplitude of Mercury and h_2.
The k-th shape measurement is then given by

$$T_k = T(\theta_k, \lambda_k + \Phi_{\mathrm{lib}} f_{\mathrm{lib}}(t_k)) + u_r(\theta_k, \lambda_k, t_k) + e_k \quad (1)$$

where θ_k, λ_k, t_k, and e_k are the co-latitude, longitude, time, and noise of the measurement, respectively. Φ_{lib} is the 88-day libration amplitude of Mercury and f_{lib} is a series expansion describing the librations. The radial tidal displacement is

$$u_r = h_2 \frac{V_2}{g} \quad (2)$$

where g is the gravitational attraction at the surface and V_2 is the second degree term of the dynamic tidal potential exerted by the Sun. In Eq. 1, T is the static global shape which is parametrized by a linear combination of 2D cubic spline functions. Each linear coefficient corresponds to a shape value on a global grid with N points. The coefficients are zero outside of the 16-neighborhood of the measurement in the grid, and higher the closer they are to the measurement location. The observation equation (Eq. 1) is solved for the N

coefficients of the basis functions, Φ_{lib}, and h_2 using non-linear least-squares and a direct sparse solver (Intel MKL PARDISO).

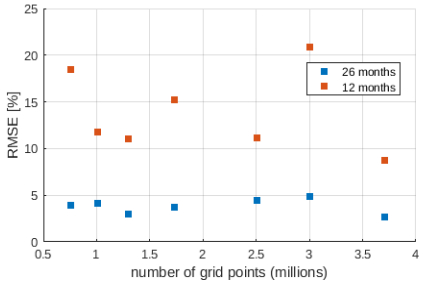

Figure 1: Dependence of the RMSE of h_2 on number of shape grid points N and the duration of the mission.

3 Results and Discussion

We compute solutions for different mission durations and different amounts of basis functions N. A large N corresponds to a high-resolution shape grid. For each combination of these two parameters, solutions are computed for different random realisations of the global shape and the noise to ensure a representative solution. The low-degree shape coefficients up to degree 50 are taken from the stereo-photogrammetric digital elevation model [1], the coefficients up to degree 1399 are simulated, and the power contained in the higher degrees is added to the nominal measurement error of 1 m. Each random realisation results in one best-fit value of h_2. We use 6 shape realisations and 9 noise realisations for each of them and take the RMSE of the resulting 54 best-fit values (Fig. 1). The highest relative accuracy is 2.7% or 8.7% for a mission duration of 26 months, corresponding to $3.3 \cdot 10^8$ measurements, or 12 months, corresponding to $1.5 \cdot 10^8$ measurements, respectively. Therefore, a large amount of measurements will be essential to retrieve h_2. The RMSE values also indicate that h_2 can generally be retrieved more accurately when the static shape is represented by a denser grid. The most accurate estimations have been performed for a $N = 3704400$ grid which has a resolution of approximately 5 km at the equator, the highest under investigation in this study. Even higher resolutions are in principle possible, but limited by the computational effort.

4. Summary and Conclusions

We have presented a method for the retrieval of the tidal Love number h_2 from laser altimetry data which is an improvement over a previous method [2]. Simulations of BELA measurements have shown that h_2 can be retrieved with a relative accuracy of 2.7% after 26 months of measurements or 8.7% after 12 months. Therefore, a large number of measurements is essential to obtain an accuracy which allows useful constraints on models of the interior structure of Mercury. The improved method can also be applied to the measurements of the Lunar Orbiter Laser Altimeter (LOLA) for validation purposes or to MLA data.

Acknowledgements

R. Thor is supported by grant 50 QW 1401 on behalf of the DLR Space Administration while preparing his PhD thesis in the framework of the International Max Planck Research School on Solar System Science at the University of Göttingen.

References

[1] Becker, K. J., Robinson, M. S., Becker, T. L., Weller, L. A., Edmundson, K. L., Neumann, G. A., Perry, M. E., Solomon, S. C.: First Global Digital Elevation Model of Mercury, Lunar and Planetary Science Conference, Vol. 47, p. 2959, 2016.

[2] Koch, C., Kallenbach, R., and Christensen, U.: Mercury's global topography and tidal signal from laser altimetry by using a rectangular grid, Planetary and Space Science, Vol. 58(14), pp. 2022-2030, 2010.

[3] Mazarico, E., Barker, M. K., Neumann, G. A., Zuber, M. T., and Smith, D. E.: Detection of the lunar body tide by the Lunar Orbiter Laser Altimeter, Geophysical Research Letters, Vol. 41(7), pp. 2282-2288, 2014.

[4] Van Hoolst, T., and Jacobs, C.: Mercury's tides and interior structure, Journal of Geophysical Research: Planets, Vol. 108(E11), 2003.

EPSC Abstracts
Vol. 11, EPSC2017-508, 2017
European Planetary Science Congress 2017

UNVEILING MERCURY's MYSTERIES WITH BEPICOLOMBO

J. Benkhoff (1), M. Fujimoto (2), G. Murakami (2) and J. Zender (1)
(1) ESA/ESTEC, SCI-S, Keplerlaan 1, 2200AG Noordwijk, Netherlands (Johannes.Benkhoff@esa.int) (2) Japan Aerospace Exploration Agency, Dept. Solar System Sci. Sagamihara Campus, Kanagawa, Japan

Abstract

NASA's MESSENGER mission has fundamentally changed our view of the innermost planet. Mercury is in many ways a very different planet from what we were expecting. Now BepiColombo [1] has to follow up on answering the fundamental questions that MESSENGER raised and go beyond.

1. Introduction

BepiColombo is a joint project between ESA and the Japanese Aerospace Exploration Agency (JAXA). The Mission consists of two orbiters, the Mercury Planetary Orbiter (MPO) and the Mercury Magneto-spheric Orbiter (MMO). The mission scenario foresees a launch of both spacecraft with an ARIANE V in October 2018 and an arrival at Mercury in 2025. From their dedicated orbits the two spacecraft will be studying the planet and its environment. The mission has been named in honor of Giuseppe (Bepi) Colombo (1920–1984), who was a brilliant Ital-ian mathematician, who made many contributions to planetary research, celestial mechanics, including the development of new space flight concepts

2. Science goals of BepiColombo

BepiColombo will study the composition, geophysics, atmosphere, magnetosphere and history of Mercury, the least explored planet in the inner Solar System. In particular, the mission objectives are: • to understand why Mercury's density is markedly higher than that of all other terrestrial planets, Moon included • to understand and determine the status of the core of Mercury, and if the planet is still tectonically active today • to understand Mercury's magnetized environment and its intrinsic magnetic field • to investigate the permanently shadowed craters of the Polar Regions • to study the production mechanisms of the exosphere and to understand the inter-action between planetary magnetic field and the solar wind in the absence of an ionosphere • to obtain new clues about the composition of the primordial solar nebula and about the formation of the solar system and • to test general relativity with improved accuracy, taking advantage of the proximity of the Sun.

In addition, the BepiColombo mission will provide a rare opportunity to collect multi-point measurements in a planetary environment. This will be particularly important at Mercury because of short temporal and spatial scales in the Mercury's environment. The foreseen orbits of the MPO and MMO will allow close encounters of the two spacecraft throughout the mission. Such intervals are very important for the inter-calibration of similar instruments on the two spacecraft.

3. Instruments

The MPO scientific payload comprises eleven instruments/instrument packages; The MMO comprises five instruments/instrument packages to study of the environment. Together, the scientific payload of both spacecraft will provide the detailed information necessary to understand Mercury and its magnetospheric environment and to find clues to the origin and evolution of a planet close to its parent star. The MPO will focus on a global characterization of Mercury through the investigation of its interior, surface, exosphere and magnetosphere. In addition, it will be testing Einstein's theory of general relativity. Major effort was put into optimizing the scientific re-turn by defining the payload complement such that individual measurements can be interrelated and complement each other. The MMO will focus on studying the environment around Mercury. The BepiColombo mission will complement and follow up the work of NASA's MESSENGER mission by providing a highly accurate and comprehensive set of observations of Mercury.

References

[1] Benkhoff, J., et al.: Planet. Space Sci. Vol.58, pp. 2-20, 2010.

EPSC Abstracts
Vol. 11, EPSC2017-521-1, 2017
European Planetary Science Congress 2017

The influence of the fluid outer core and of the solid inner core on the orientation of the rotation axis of Mercury

R.-M. Baland, M. Yseboodt, T. Van Hoolst and A. Rivoldini
Royal Observatory of Belgium, Ringlaan 3, B-1180 Brussels, Belgium (rose-marie.baland@oma.be)

Abstract

Mercury's spin axis nearly occupies an equilibrium state in which the orbit normal and spin axis precess together with a long period of about 300 000 years. We develop a Cassini state model for the equilibrium orientation of the spin axis of Mercury's mantle that takes into account all the effects of pericenter precession, tidal deformations, and couplings between internal layers, including dissipative core-mantle boundary viscous coupling. Such an extended model will be useful for the interpretation of future BepiColombo rotation measurements.

1. Introduction

Mercury's spin axis nearly occupies the Cassini state 1, in which the orbit normal and spin axis precess together with a long period of about 300 000 years. Mercury slightly deviates from that state which is defined for a uniformly precessing rigid planet. The slow precession of the pericenter (period of about 127 000 years) induce variations in obliquity and deviation from the coplanarity between the spin axis, the normal to the orbit and the normal to the Laplace plane, while the short-periodic tidal deformations induce a constant shift over time in mean obliquity and deviation [2].

Measurements of tides [5, 10] and of the longitudinal librations at a period of 88 days [3, 4] indicate that the core of Mercury is at least partially liquid, decoupling the solid mantle and crust from the interior. Peale et al. (2014, 2016) have shown that the internal torques resulting from the presence of a fluid outer core and a solid inner core might increase the equilibrium obliquity and lead to an overestimate of the polar moment of inertia from the measured obliquity [6, 7].

Here, we develop a Cassini state model for the equilibrium orientation of the mantle spin axis that takes into account all the effects of pericenter precession, tidal deformations, conservative torques related to the presence of an outer fluid core and of an inner solid core, dissipative core-mantle boundary viscous coupling.

2. Methodology

We consider three-layer interior models with a silicate shell (consisting of mantle and crust), a liquid outer core and a solid inner core. Those models are constrained by the mass, radius, second-degree gravity field coefficients and libration amplitude [9].

We express the spin axis motion in a frame based on the Laplace plane [1]. We take into account the solar gravitational torque exerted on each layer, the internal gravitational torques between the internal layers and the pressure torques as well as the dissipative viscous torques exerted at the interfaces. We include the effect of tidal periodic deformations and of pericenter precession on each layer, by generalizing the developments for a solid Mercury [2].

We use the extended Cassini state model to reinterpret recent determination of Mercury's orientation (e.g. Stark et al. 2015 [8]) in terms of parameters of Mercury's interior, particularly the polar moment of inertia and the tidal quality factor, and evaluate potential improvements with future data by the BepiColombo mission.

Acknowledgements

The research leading to these results has received funding from the Belgian PRODEX program managed by the European Space Agency in collaboration with the Belgian Federal Science Policy Office.

References

[1] Baland, R.-M., Yseboodt, M., Van Hoolst, T., 2016. The obliquity of Enceladus. Icarus, Vol. 268, p. 12-31.

[2] Baland, R.-M., Yseboodt, M, Rivoldini, A., Van Hoolst, T., 2017. Obliquity of Mercury: Influence of the preces-

sion of the pericenter and of tides. Icarus, Vol. 291, p. 136-159.

[3] Peale, S. J., Margot, J.-L., Hauck, S. A., Solomon, S. C., 2014. Effect of core-mantle and tidal torques on Mercury's spin axis orientation. Icarus, Vol. 231, p. 206-220.

[4] Peale, S. J., Margot, J.-L., Hauck, S. A., Solomon, S. C., 2016. Consequences of a solid inner core on Mercury's spin configuration. Icarus, Vol. 264, p. 443-455.

[5] Mazarico, E., Genova, A., Goossens, S., Lemoine, F. G., Neumann, G. A., Zuber, M. T., Smith, D. E., Solomon, S. C., 2014. The gravity field, orientation, and ephemeris of Mercury from MESSENGER observations after three years in orbit. Journal of Geophysical Research (Planets), Vol. 119. p. 2417-2436.

[6] Margot, J. L., Padovan, S., Peale, S. J., Solomon, S. C., 2011. Measurements of Mercury's spin state and inferences about its interior. Abstract P41A-1573, paper presented at the American Geophysical Union Fall Meeting, San Francisco, CA, 5 to 9 December 2011.

[7] Margot, J. L., Peale, S. J., Solomon, S. C., Hauck, II, S. A., Ghigo, F. D., Jurgens, R. F., Yseboodt, M., Giorgini, J. D., Padovan, S., Campbell, D. B., 2012. Mercury's moment of inertia from spin and gravity data. Journal of Geophysical Research (Planets), Vol. 117, E00L09.

[8] Stark, A., Oberst, J., Preusker, F., Gwinner, K., Peale, S. J., Margot, J.-L., Phillips, R. J., Zuber, M. T., Solomon, S. C., 2015. First MESSENGER orbital observations of Mercury's librations. Planetary and Space Science, Vol. 117, p. 64-72.

[9] Rivoldini, A., Van Hoolst, T., 2013. The interior structure of Mercury constrained by the low-degree gravity field and the rotation of Mercury. Earth and Planetary Science Letters, Vol. 377, p. 62-72.

[10] Verma, A. K., Margot, J.-L., 2016. Mercury's gravity, tides, and spin from MESSENGER radio science data. Journal of Geophysical Research (Planets), Vol. 121, p. 1627-1640.

EPSC Abstracts
Vol. 11, EPSC2017-526, 2017
European Planetary Science Congress 2017

Determination of Mercury's gravity and orientation through the BepiColombo's radio science experiment

M. J. Mariani and L. Iess
(1) Sapienza University of Rome, Italy (mircojunior.mariani@uniroma1.it)

Abstract

The Mercury Orbiter Radio science Experiment (MORE) is one of the investigations of the ESA/JAXA BepiColombo mission to Mercury. MORE is designed to estimate the Mercury's gravity field, its rotational state, and to perform tests of relativistic gravity. The state-of-the-art onboard and ground instrumentations enables simultaneous two-way links in X/X, X/Ka, and Ka/Ka, providing a range rate accuracy of 3 micron/s (at 1000 s of integration time) and range accuracy of 20 cm. The non-gravitational acceleration will be provided by a dedicated accelerometer (Italian Spring Accelerometer, ISA). We present the results of the numerical simulations of the Mercury's gravity field and orientation recovery. They were carried out considering the latest mission scenario and including the ISA in-flight calibration in the orbit determination process to reduce measurement errors due to electronic noise, thermal drift, and ageing.

1. Introduction

The European Space Agency (ESA) and the Japanese Space Exploration Agency (JAXA) are developing the dual-spacecraft mission BepiColombo to survey and explore the planet Mercury. The mission is scheduled for launch in October 2018, with arrival in Mercury in December 2025. Due to gravitational perturbations the orbit will undergo significant changes, with an increase of the eccentricity and a latitudinal precession of the pericenter. One of the two spacecraft, the Mercury Planetary Orbiter (MPO), will be devoted to the study of the internal structure of Mercury and its surface geology. The MPO will have a near-polar orbit with pericenter at 480 km and apocenter at 1500 km and will host the Mercury Orbiter Radio science Experiment (MORE). MORE consists of a radio tracking system that supports multi-frequency radio links in X- and Ka-band between the spacecraft and ground stations. Range rate and range measurements, accurate respectively to 3 μm/s (at 1000 s time scale) and 20 cm at nearly all elongation angles, will be collected to reconstruct the spacecraft orbit and to estimate Mercury's gravity field, its pole orientation parameters (right ascension and declination of the pole), and the amplitude of librations in longitude [1]. Non-gravitational accelerations, quite large at Mercury (about 10^{-6} m/s^2), will be removed to a large extent using the accelerometer data provided by the Italian Spring Accelerometer (ISA).

2. End-to-End simulation of MORE experiment

We simulated the two-way Doppler and range data accounting for station visibility (we used two ground antennas, at Goldstone and Cebreros) and operational constraints due to the pointing of the moveable High Gain Antenna (HGA). These data were processed in in batches 24 h long using JPL MONTE code and software developed in house to integrate the trajectory and carry out the orbital fit. The mathematical formulation is based on [2]. We also modeled the reaction wheels' desaturation maneuvers twice a day that produce uncompensated ΔVs of about 70 mm/s and we simulated and included the ISA acceleration measurements to recover the MPO orbit. The accelerometer error is composed by a random noise, systematics, and biases. In the instrument measurement band, (3×10^{-5}-10^{-1} Hz), the intrinsic random noise decreases from 8×10^{-8} $m/s^2/Hz^{1/2}$ at 3×10^{-5} Hz to 7×10^{-8} $m/s^2/Hz^{1/2}$ at 7×10^{-4} Hz, then remains constant up to 10^{-1} Hz. The main systematic errors evolve periodically following MPO's orbital period and half of Mercury's orbital period. The amplitude of the 44-days error is 4.2×10^{-8} m/s^2. This error can be calibrated by means of a daily bias and bias-rate estimation. The amplitude of the orbital error is 7×10^{-9} m/s^2 for the ISA proof masses in radial and cross-track direction, and 3×10^{-9} m/s^2 in the along-track direction. The ISA scale factors error is due to the effect of the thermal hysteresis and can be assumed constant and equal to 10^{-2}. The a priori Mercury's gravity field and tidal Love number k_2 ware taken by the HgM005 solution derived from

MESSENGER radio data [3]. The assumed Mercury's orientation parameters are based on Margot's recommended model, including the librations in longitude [4]. The parameters of interest were estimated applying a multiarc method by means of square root information, weighted, least-squares filter. The global solve-for parameters are the gravity field in spherical harmonic to degree and order 30, the pole orientation, the amplitude of the libration in longitude, and the ISA scale factor. The local solve-for parameters are the spacecraft position, the velocity, the ISA bias, its drift, the amplitude of ISA error at orbital period and the ΔV of desaturation maneuvers. We simulated the 1-year of MORE operations in orbit about Mercury demonstrating that the scientific goals of the gravimetry experiment will be met. The attainable accuracies are in of about $1x10^{-11}$ for the degree 2 field and about 5×10^{-9} for the degree 30.

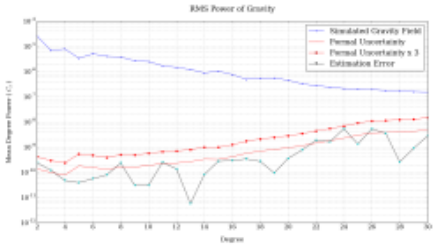

Figure 1: Power spectrum of Mercury's gravity field with estimation error and formal uncertainty.

Despite the introduction of dynamical perturbations and initial errors in the dynamical model, the results meet the science requirement of MORE. The k_2 Love number and the amplitude of 88-days longitudinal libration are determined with formal uncertainties of 3.2×10^{-4} and 0.2", respectively. The right ascension and the declination of Mercury's pole are estimated at the level of 0.32" and 0.11". The reconstructed trajectories provide uncertainty of < 30 cm in the radial direction that will allow a well referencing of the altimetry observations from the BELA laser altimeter. For all estimated parameters, the estimation error remains in the range between one and three formal uncertainty.

3. Summary and Conclusions

The results of the simulation of the gravity and rotation experiment using radio tracking observable and accelerometer data indicate that BepiColombo will provide a global determination of Mercury's gravity field meeting and exceeding the science requirements of the mission. These goals will be attained thanks to the state of the art radio tracking system in Ka-band and the ISA accelerometer. The MORE experiment will improve the knowledge of Mercury's gravity field in the equatorial region and in the southern hemisphere. The MPO spacecraft will cover Mercury's regions at low altitudes (200-500 km) where MESSENGER had poor sensitivity because of its highly eccentric orbit.

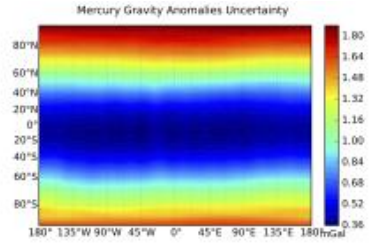

Figure 2: Gravity anomalies uncertainty obtained by the gravity field (30x30) covariance.

Acknowledgements

This work was supported in part by the Italian Space Agency (ASI).

References

[1] Iess, L., Asmar, S., Tortora, P., "MORE: An advanced tracking experiment for the exploration of Mercury with the mission BepiColombo", Acta Astronautica 65, pp. 666–675, Sep. 2009

[2] Moyer, T. D.: Formulation for Observed and Computed Values of Deep Space Network Data Types for Navigation, Wiley, 2005.

[3] Mazarico, E., et al.: The gravity field, orientation, and ephemeris of Mercury from MESSENGER observations after three years in orbit, J. Geophys. Res. Planets, 119, 2417–2436, doi:10.1002/2014JE004675.

[4] Margot J.-L.: A Mercury orientation model including non-zero obliquity and librations, Celest Mech Dyn Astr (2009) 105: 329. doi:10.1007/s10569-009-9234-1

EPSC Abstracts
Vol. 11, EPSC2017-535, 2017
European Planetary Science Congress 2017

A time-averaged regional model of the Hermean magnetic field

E. Thébault (1), B. Langlais (1), J.S. Oliveira (2), H. Amit (1), and L. Leclercq (3)
(1) Laboratoire de Planétologie et de Géodynamique de Nantes, Université de Nantes, France
(2) Institut de Physique du Globe de Paris, Sorbonne Paris Cité, France
(3) University of Virginia, Charlottesville, VA, USA

Abstract

This paper presents the first regional magnetic field model of Mercury developed with mathematical continuous functions. The model is derived to the spatial resolution of about 830 km without a priori information about the geometry of the internal and external fields or regularization. It relies on an extensive dataset of the MESSENGER's measurements selected over its entire orbital lifetime between 2011 and 2015. A first order separation between the internal and the external fields over the Northern hemisphere is achieved under the assumption that the magnetic field measurements are acquired in a source free region within the magnetospheric cavity. When downward continued to the core-mantle boundary, the model confirms the general structures already observed in previous studies such as the dominance of zonal field, the location of the North magnetic pole, and the global absence of significant small scale structures. The transformation of the regional model into a global spherical harmonic one provides an estimate for the axial quadrupole to axial dipole ratio of about g20/g10=0.27. This is much lower than previous estimates of about 0.40. We however note that it is possible to obtain a similar ratio provided that more weight is put on the location of the magnetic equator and less elsewhere.

1. Introduction

One of the objectives of the MESSENGER spacecraft was to better describe the magnetic fields surrounding the planet Mercury and to better understand their origin. The magnetic measurements are acquired by MESSENGER along a near polar but very elliptical orbit and are useful for internal magnetic field studies mostly above the northern hemisphere. This orbital configuration challenges our ability to separate the measured magnetic fields into their internal and external contributions and to model them globally to high spatial resolution using classical mathematical techniques such as the spherical harmonics ([1], [2]).

In the recent years, attempts have been made to circumvent this difficulty using dedicated regional or local techniques. Such techniques could rely on an equivalent representation of sources (e.g. [3]) using hypotheses about the location of the magnetic field sources. However, other techniques inherited from Earth’s studies based on regional mathematical functions could equally be applied without the need for a priori information about the sources. In this paper, we apply the Revised Spherical Cap Harmonic Analysis ([4]) to derive a magnetic field model from the magnetic field measurements of the MESSENGER spacecraft.

2. Model and results

We use the latest MESSENGER calibrated magnetic field measurements (MESSENGER Data Release 15, version V08) acquired during more than 8 Mercury solar days from 23 March 2011 until 30 April 2015. We apply a proxy defined by [3] to identify and select for each orbit the measurements within the magnetospheric cavity and below 1000 km altitude. This maximum altitude aims at excluding data too close to the day side magnetopause that may have large spatio-temporal variability. The selected orbit portions correspond to reduced external field perturbations. The selected data are confined within a cone of 85° half-aperture. The cone is aligned onto Mercury's axis of rotation and covers almost the entire Northern hemisphere. A full azimuthal coverage in the Mercury Body Fixed (MBF) coordinate system is completed every sidereal day on Mercury (about 56 Earth's days). The geographical coverage within the cone in the MBF reference frame

is therefore very dense. Due to the spin orbit 3:2 resonance on Mercury, all MLT are surveyed after 3 days or 2 years, which corresponds to 1 solar day. The coverage in MLT is sufficient to average out (in principle) the external field contributions which are more or less static in the Mercury-centric Solar Orbital (MSO) reference frame. The median and mean altitudes of the measurements are 500 and 530 km, respectively. The radial distribution is dense, but the low latitude measurements are at higher altitudes, with a median altitude equal to 700 and 450 km south and north of 45. This data selection protocol generates a dataset of 1,675,748 data triplet (5,141,166 vector field components).

The magnetic field is strongly axisymmetric. The North dip pole is located at 87N;94W. The most striking feature in the maps is the absence of small scale structures at the CMB. This observation is not novel but relied so far on SH models truncated to very low degrees and orders. The magnetic equator is found around latitude 14.9°N at 200 km altitude and at about 11.5N at 1000 km altitude. This latter estimation is consistent with the average location of the solar wind standoff distance at Mercury estimated to be at 1.41 Mercury's radius [2]. We finally transform the regional model into a truncated global SH model. We estimate only the low degree coefficients that are the least correlated over the northern hemisphere and compare the coefficients to those published by [1].

Table 1: Comparison between the SH model coefficients obtained in this paper and the model of [1]

Coefficients	This paper	Model of [1]
g_1^0	-213.6	-190.0
g_1^1	0.9	n/a
h_1^1	1.5	n/a
g_2^0	-57.7	-74.6
g_3^0	-35.8	-22.0
g_5^0	2.1	n/a

3. Summary and Conclusions

Our results illustrate that if the co-estimation of the zonal internal quadrupole and the external dipole terms are important to preserve the most robust features detected by the MESSENGER's measurements, an alternative picture of Mercury's magnetic field can be obtained in SH by relaxing this constrain. In such a case, the axial quadrupole to axial dipole ratio is significantly reduced from 0.4 to 0.27. This result could broaden the class of acceptable dynamo regimes for Mercury by perhaps alleviating the need for heterogeneous heat flux at the CMB. The model of Anderson et al. [1] is therefore probably a suitable model to estimate the location of the magnetic dip pole at altitudes larger than 800 km with few SH parameters but seems not optimal for representing the magnetic field in the lower altitude range, particularly at the CMB. However, even if the SH model presented in this paper is by construction currently uncertain, the regional model downward continued to the CMB could represent an attractive alternative to constrain dynamo simulations.

Acknowledgements

This work is partly funded through the ANR project MARMITE (ANR-13-BS05-0012)

References

[1] Anderson, B. J., Johnson, C. L., Korth, H., Winslow, R. M., Borovsky, J. E., Purucker, M. E., ... & McNutt, R. L. (2012). Low‐degree structure in Mercury's planetary magnetic field. Journal of Geophysical Research: Planets (1991–2012), 117(E12).

[2] Johnson, C. L., Purucker, M. E., Korth, H., Anderson, B. J., Winslow, R. M., Al Asad, M. M., ... & Solomon, S. C. (2012). MESSENGER observations of Mercury's magnetic field structure. Journal of Geophysical Research: Planets (1991–2012), 117(E12).

[3] Oliveira, J. S., Langlais, B., Pais, M. A., & Amit, H. (2015). A modified Equivalent Source Dipole method to model partially distributed magnetic field measurements, with application to Mercury. Journal of Geophysical Research: Planets, 120(6), 1075-1094.

[4] Thébault, E., Schott, J. J., & Mandea, M. (2006). Revised spherical cap harmonic analysis (R‐SCHA): Validation and properties. Journal of Geophysical Research: Solid Earth (1978–2012), 111(B1).

EPSC Abstracts
Vol. 11, EPSC2017-591, 2017
European Planetary Science Congress 2017

High-resolution topography from MESSENGER orbital stereo imaging – The Southern hemisphere

F. Preusker (1), J. Oberst (1,2), A. Stark (1), K.-D. Matz (1), K. Gwinner (1) and T. Roatsch (1)

(1) German Aerospace Center, Institute of Planetary Research, Department of Planetary Geodesy, D-12489 Berlin, Germany (Frank.Preusker@dlr.de), (2) Technical University Berlin, Institute for Geodesy and Geoinformation Sciences, Berlin, Germany

1. Introduction

The MErcury Surface, Space ENviorment, GEochemistry, and Ranging (MESSENGER) spacecraft entered orbit about Mercury in March 2011 [1] to carry out a comprehensive topographic mapping of Mercury. Measurements of Mercury's topography have been made with stereo imaging [2,3], laser altimetry [4], limb profiling [5], and radio occultation [6]. We are concerned with the production of high-resolution digital terrain models (DTM) using stereo photogrammetry. While we recently reported about the production and delivery of DTMs for the northern quadrangles H6 "Kuiper" [7], H3 "Shakespeare", H5 "Hokusai", and H7 "Beethoven" [8-10], we now report about the status of Mercury's Southern hemisphere quadrangles (Fig. 1).

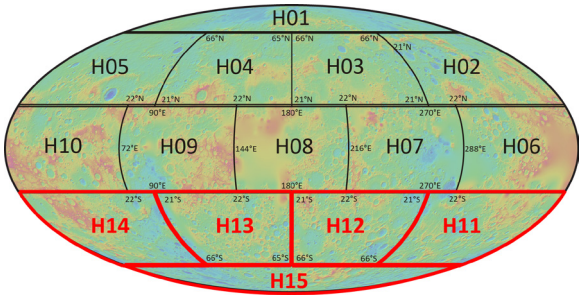

Figure 1: Mercury's 15 tiles quadrangle scheme. The selected Southern hemisphere quadrangles H11 – H15 are highlighted in red.

2. Data

The Mercury Dual Imaging System (MDIS) onboard MESSENGER spacecraft consists of a wide-angle camera (WAC) and a narrow-angle camera (NAC) co-aligned on a pivot platform. In almost 4 years MDIS has acquired more than 200,000 images to map the surface. Owing to MESSENGER's highly eccentric near-polar orbit, the WAC is primarily used for the northern hemisphere and the NAC to cover the southern hemisphere, respectively.

3. Method

The stereo-photogrammetric processing for Mercury is based on a software suite that has been developed within the last decade and has been applied successfully to several planetary image data sets. The suite comprises photogrammetric block adjustment, multi-image matching, surface point triangulation, DTM generation, and base map production.

4. Results

Each quadrangle tile contains between 8000 and 15,000 individual images. Approximately 105,000 images have been used to date. We first corrected for errors in the nominal navigation (pointing and position) data using a photogrammetric block adjustment. This step improved the three-dimensional (3D) point accuracy in all tiles from about ±800 m to about ±50 m. Next, individual image matching runs were carried out to produce tens of billion object points (surface points). The mean ray intersection error of the surface points was ±50 m. Only triple-overlapping images were used for the matching. Then, we generated a DTM for each tile with a lateral spacing of 192 pixel per degree (~222 m/pixel) and a vertical accuracy of about 50 m (Fig. 2.). Finally we will merge all DTMs.

Acknowledgements

The MESSENGER project is supported by the NASA Discovery Program under contracts NASW-00002 to the Carnegie Institution of Washington and NAS5-97271 to The Johns Hopkins University Applied Physics Laboratory. We thank MESSENGER's MLA and MDIS team members for their support, especially Susan Ensor, Haje Korth, Erwan Mazarico, Gregory Neumann, Michael Reid, and Sean Solomon.

References

[1] Solomon S.C et al.: Mercury after six months of MESSENGER orbital observations, EPSC-DPS Joint Meeting Abstracts and Program, abstract EPSC-DPS2011-430, 2011.

[2] Oberst J. et al.: The morphology of Mercury's Caloris basin as seen in MESSENGER stereo topographic models, Icarus, 209, 230–238, 2010.

[3] Preusker F. et al.: Stereo topographic models of Mercury after three MESSENGER flybys, Planet. Space Sci., 59, 1910–1917, 2011.

[4] Zuber, M.T. et al.: Topography of the Northern Hemisphere of Mercury from MESSENGER Laser Altimetry, Science, 336, 217-220, 2012.

[5] Elgner S. et al.: Mercury's global shape and topography from MESSENGER limb images, Planet. Space Sci., 103, 299-308, 2014.

[6] Perry M.E. et al.: Measurement of the radius of Mercury by radio occultation during the MESSENGER flybys, Planet. Space Sci., 59, 1925-1931, 2011.

[7] Preusker et al. et al.: Toward High-Resolution Global Topography of Mercury from MESSENGER Orbital Stereo Imaging: A Prototype Model for the H6 (Kuiper) Quadrangle, Planet. Space Sci., in press, 2017.

[8] Preusker et al. et al.: High-Resolution Topography from MESSENGER Orbital Stereo Imaging – The H3 quadrangle „Shakespeare", LPSC, 48, 1441, 2017.

[9] Stark et al. et al.: High-Resolution Topography from MESSENGER Orbital Stereo Imaging – The H5 quadrangle „Hokusai", LPSC, 48, 2287, 2017.

[10] Oberst et al. et al.: High-Resolution Topography from MESSENGER Orbital Stereo Imaging – The H7 quadrangle „Beethoven", LPSC, 48, 1442, 2017.

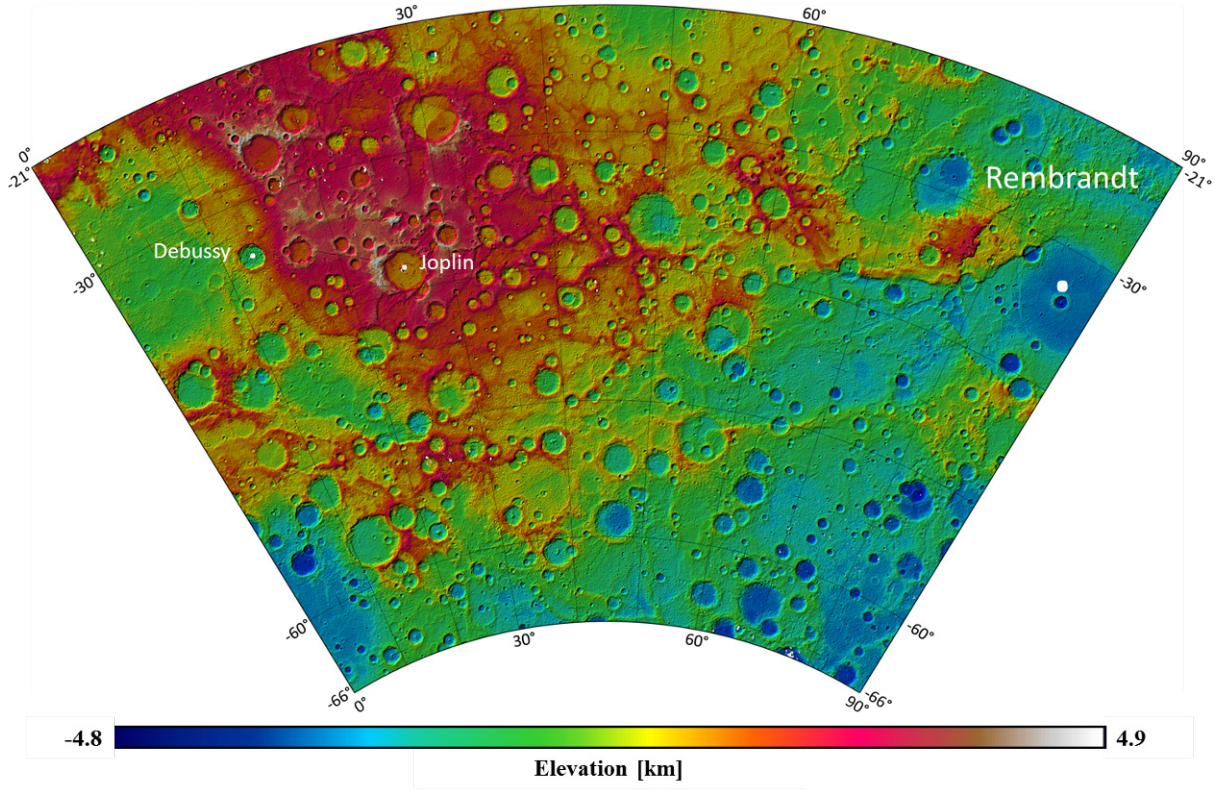

Fig. 2. H14 ("Debussy") quadrangle DTM (hill-shaded color-coded heights) with a lateral spacing of 192 pixel per degree (~222 m) in Lambert two-parallel (conformal) projection.

EPSC Abstracts
Vol. 11, EPSC2017-610, 2017
European Planetary Science Congress 2017

Emissivity Spectra of Mercury Analogues under Mercury Pressure and Temperature Conditions

A. Maturilli, J. Helbert, I. Varatharajan and M. D'Amore
Institute for Planetary Research, German Aerospace Center DLR, Rutherfordstr. 2, 12489 Berlin, Germany – alessandro.maturilli@dlr.de

Abstract

The MERTIS (MErcury Radiometer and Thermal infrared Imaging Spectrometer) instrument onboard the ESA/JAXA BepiColombo mission (launch is scheduled for 2018) is designed to identify rock-forming minerals, to map the surface composition, and to study the surface temperature variations with an uncooled microbolometer detector in the hot environment of Mercury. MERTIS is an advanced IR instrument combining a push-broom IR grating spectrometer (TIS) with a radiometer (TIR) sharing the same optics, instrument electronics and in-fight calibration components for a wavelength range of 7-14 and 7-40 µm, respectively.

At the Planetary Spectroscopy Laboratory (PSL) we measured emissivity spectra in vacuum (0.7 mbar) for a large suite of Mercury surface analogue materials in the MERTIS spectral range (7-14 µm) for sample temperatures from 100°C to above 400°C.

1. Introduction

At PSL, two identical FTIR instruments (Bruker Vertex 80V) are operating in an air-conditioned room. One spectrometer is equipped with aluminum mirrors optimized for the UV, visible and near-IR, the second features gold-coated mirrors for the near to far IR spectral range. An external chamber is attached to the second spectrometer to measure the emissivity of solid samples. A shutter allows separating the spectrometer from the external chamber, which can be evacuated to the same pressure as the spectrometer. If needed, an optical window (vacuum tight) can be mounted at the entrance of the emissivity chamber to operate while keeping the external chamber at ambient pressure under purged air or under inert gases. Sample targets are brought to measuring temperature using an induction heating system. For this reason our sample cups and heating surfaces are made of stainless steel. Our high efficiency induction system heats the samples to temperatures from 320K up to 900K. A sample caroussel driven by a very precise stepper motor (computer controlled) allows measuring several consecutive samples without breaking the vacuum. A large number of temperature sensors in the emissivity chamber allow monitoring the temperature of the sample as well as of several points at the equipment and chamber. A webcam is mounted in the emissivity chamber to monitor the heated sample and its vicinity. For more details, see [1, 2, 3, 4].

2. Mercury Analogues Collection

Most recent results from MESSENGER's X-Ray Spectrometer, Gamma-Ray Spectrometer, and Neutron Spectrometer [5] have been used to compile the list of Mercury analogues. Average surface composition falls very close to the komatiite–boninite boundary. The surface of Mer-cury is mainly composed of Mg-rich orthopyroxene and plagioclase; plagioclase and orthopyroxene dominate the surface materials, with lesser amounts of clinopyroxene, sulfides, olivine, and silica (at lower abundances than olivine). Our collection of analogues contains olivine, enstatite, labradorite, augite, komatiite (see [6]), tektite, anorthoclase, bytownite, L-chondrite, albite, hypersthene, diopside, quartz, nepheline, graphite, a lunar simulant JSC-1A, and many sulfides. Emissivity spectra of sulfides in particular are described in [7].

3. Emissivity Measurements

Mercury regolith is mostly composed of very fine particles, therefore we selected the samples to be measured from our collection in the smaller fraction, being < 25 µm. Each sample was poured in a stainless steel cup and placed in the external emissivity chamber, in a position ready for measurement. Temperature sensors were put in contact with the sample emitting layer and with the sample cup, to monitor its heating properties. The emissivity chamber was then evacuated and when

stable vacuum was reached (0.7 mbar), the induction system was switched on for heating the samples. Each sample was carefully and slowly heated to reach 100°C, 200°C, 300°C, and 400°C, with different sample surface temperature simulating different insulation properties (time of day and/or latitude) on Mercury surface.

4. Spectral Collection

In the wavelength range (7-14 µm) which will be investigated by the MERTIS spectrometer, several very diagnostic spectral features can be identified. Their evolution with surface temperature (that can also be predicted and modeled) have been already described in many scientific publications [3, 8, 9]. In this paper we show the emissivity spectra measured for 2 endmembers of the Mercury analogue collection, at the 4 already described increasing surface temperatures: komatiite from Barberton (Fig.1), and olivine (Fig. 2), all of them in the size fraction < 25 µm.

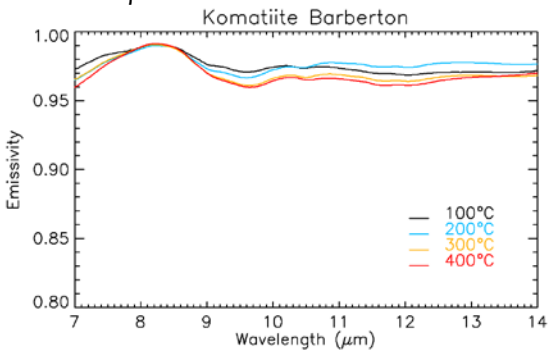

Figure 1. Emissivity spectra for a Barberton komatiite < 25 µm, measured at PSL.

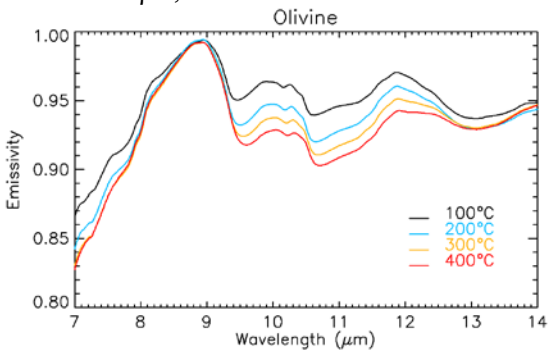

Figure 2. Emissivity spectra for an olivine ($Fo_{\#89}$) < 25 µm, measured at PSL.

These 2 entries show the strong diagnostic capabilities of the spectral signatures characteristic for the MERTIS spectral range: one can see variations in the position and shape on the CF (emissivity maxima) below 9 µm, in the shape of the Reststrahlen band (9-11 µm), and in that of the Transparency region (around 12 µm) for the 3 different materials, and the temperature dependence of some of them (c.f. the Reststrahlen bands for olivine [9]).

5. Conclusions and outlook

MERTIS on Bepicolombo will be the first spectrometer to observe the hot surface of Mercury in the thermal infrared wavelength range (7-14 µm), where very diagnostic features will help the detection of minerals composing the Hermean surface. These features are temperature dependent to a varying degree, therefore their spectral behavior is influenced by local insolation conditions. To prepare an adequate spectral database for MERTIS, at the Planetary Spectroscopy Laboratory (PSL) we measured emissivity spectra in vacuum for a large suite of Mercury surface analogue materials for sample temperatures from 100°C to above 400°C. The spectral library for Mercury analogues is completed by reflectance measurements on the same samples, fresh and after been heated in vacuum, covering the whole spectral range from 0.2 to 200 µm.

References

[1] Maturilli, A. and Helbert, J.: PSS, Vol. 54, pp. 1057-1064, 2006.
[2] Maturilli, A., Helbert, J., and Moroz L., PSS, Vol. 56, pp. 420-425, 2008, spectral library now available http://figshare.com/articles/BED_Emissivity_Spectral_Library/1536469.
[3] Helbert, J. and Maturilli, A., EPSL, Vol. 285, pp. 347-354, 2009.
[4] Maturilli A, Helbert J., Journal of Applied Remote Sensing, Vol 8, 2014.
[5] Vander Kaaden, K. et al. (2016) doi: 10.1016/j.icarus.2016.11.041
[6] Maturilli A., Helbert J., St. John J.M., Head III J.W., Vaughan W.M., D'Amore M., Gottschalk M., Ferrari S., EPSL, Vol. 398, pp. 58-65, 2014.
[7] Varatharajan, I. et al., this meeting.
[8] Helbert, J. et al. (2013) doi:10.1016/j.epsl.2013.03.038.
[9] Ferrari, S., F. Nestola, M. Massironi, A. Maturilli, J. Helbert, M. Alvaro, M. C. Domeneghetti and F. Zorzi (2014) American Mineralogist 99(4): 786-792.

EPSC Abstracts
Vol. 11, EPSC2017-682, 2017
European Planetary Science Congress 2017

Bepicolombo Laser Altimeter (BELA) contributions to MPO orbit improvement towards a better determination of Mercury geophysical parameters

A. Hosseiniarani (1), S. Bertone(2), A. Jäggi(2), N. Thomas(1)
(1) Physics Institute, University of Bern, Switzerland (seyedalireza.hosseiniarani@space.unibe.ch / Tel: +41-31-6314214),
(2) Astronomical Institute, University of Bern, Switzerland

Abstract

Laser altimetry is the main source of information to improve planetary topography. However, it is also possible to use it in the form of crossovers to significantly improve the spacecraft orbit [1] and infer geophysical properties [2, 3]. In this study we will present our latest results on modeling BELA instrument [4] in flight and the potential improvement of MPO orbit. The impact of using altimetry crossovers on Mercury geophysical parameters is one of the final goals of this study and will be the object of future talks.

1. Introduction

BepiColombo is Europe's first mission to Mercury [5]. It will set off in 2018 on a journey to the smallest and least explored terrestrial planet in our Solar System, Mercury. When it arrives, it will study and understand the composition, geophysics, atmosphere, magnetosphere and history of the planet. The mission comprises two spacecraft: the Mercury Planetary Orbiter (MPO) and the Mercury Magnetospheric Orbiter (MMO). The BepiColombo Laser Altimeter (BELA) is one of the instruments of MPO and is being developed by a consortium led by Physikalisches Institut, Universitat Bern and the DLR Institute of Planetary Research Berlin. It will provide an accurate digital terrain model and improve our knowledge about the geophysical parameters of the planet Mercury.

2. The model of the instrument in flight

To know the possible scientific developments that can be achieved using BELA, we need to have a model of the instrument in flight. In our orbit propagation, we use the d/o 50 gravity field Hgm005 (derived from NASA Messenger data) as background field. Moreover, we model the gravitational effect of the Sun and of other planets on the orbit of MPO. We also assume a cannonball model for the spacecraft to take into account the effect of solar radiation pressure. A more accurate macromodel of MPO and the effect of IR radiation and albedo from the surface of Mercury on the orbit of the spacecraft are being implemented to improve the quality of our simulation. With these assumptions, the MPO orbit has been propagated and verified against orbits provided by DLR and ESA as shown in Fig. 1. Here we present our latest model which has been developed using the planetary extension of the Bernese GNSS Software (BSW [6]). The latter is an advanced space data processing software developed at the Astronomical Institute of the University of Bern (AIUB).

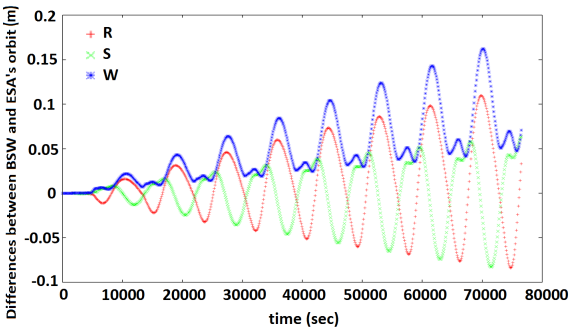

Figure 1: Orbit differences between BSW propagation and ESA SPK orbit, not exceeding 15 cm over 1 day.

To model the BELA instrument within our simulation, we use the end-to-end test results of BELA calibration in the "Starsim" laboratory of the University of Bern. Hence, to test our instrument in flight model, we simulate a series of laser altimetry observations around Mercury based on a full coverage Mercury DTM from Messenger camera data [7] and we add both random and systematic errors to the observables to have a real-

istic simulation. An example of our simulation results is shown in Fig. 2.

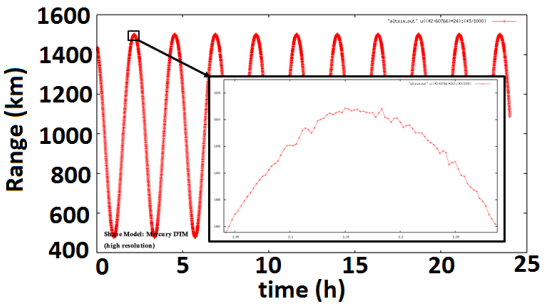

Figure 2: Measured range as a function of time in altimetry simulations.

3. Study of the orbit improvement using laser altimetry

An accurate orbit determination for MPO can be performed by using data from radio tracking. Cicalò et al [8] modelled range and range-rate data from MORE (Mercury Orbiter Radio science Experiment) Ka-band antenna and showed that it is possible to reconstruct the orbit with an accuracy of the order of one meter. Since the amplitude of Mercury tidal deformations is in the order of less than one meter, their determination will benefit from a more accurate orbit. Therefore, we study the impact of using laser altimetry observations as additional contribution to the orbit improvement as well as to the determination of other geophysical parameters. For this study, we simulate both Doppler and laser altimetry data based on MPO nominal orbit (see Fig. 3) and we reconstruct the orbit using both observation types with an appropriate weighting. Then, we compare the results to both the nominal orbit and the one only based on Doppler observations. We will present our latest advances on this topic.

4. Summary and Conclusions

We modelled the orbit of the MPO spacecraft and simulated the Doppler and laser altimetry observations to study the impact of using laser altimetry on orbit determination. We present our latest advances on this topic, including sensitivity studies w.r.t. the impact of uncertainties on Mercury gravity field, non-gravitational forces ($e.g.$, solar radiation pressure) and instrument related noises. The final goal of this study is to contribute to improve the determination of Mercury geophysical parameters ($e.g.$, tidal deformations and librations).

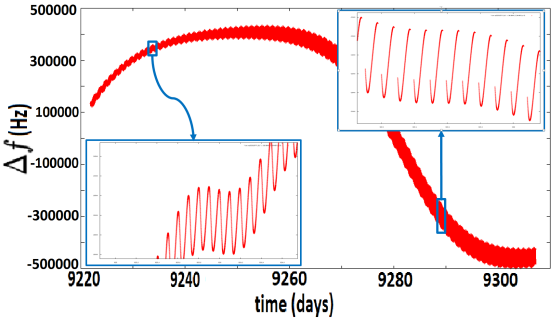

Figure 3: Simulated Doppler observation of MPO spacecraft as a function of time.

Acknowledgements

This study has been funded with the support of the Swiss National Foundation (SNF) and NCCR PlanetS.

References

[1] Rowlands D.D. et al: The Use of Laser Altimetry in the Orbit and Attitude determination of Mars Global Surveyor, GRL, 1999

[2] Stark A. et al: Mercury's Rotation Rate from Three Years of Observations by the Mercury Laser Altimeter, 46th LPSC, 2015

[3] Rosat, S. et al: Mars and Mercury rotation variations from altimetry crossover data: Feasibility study. JGR, 2008

[4] Thomas, N. et al: The BepiColombo Laser Altimeter (BELA): Concept and baseline design, PSS, 2007

[5] Benkhoff, J. et al: BepiColombo—Comprehensive exploration of Mercury: Mission overview and science goals, PSS, 2010

[6] Dach, R. et al: Bernese GNSS Software Version 5.2. AIUB, 2015.

[7] Courtesy USGS Astrogeology Science Center, http://astrogeology.usgs.gov

[8] S. Cicalò et al: The BepiColombo MORE gravimetry and rotation experiments with the ORBIT14 software, MNRAS, 2016.

EPSC Abstracts
Vol. 11, EPSC2017-753, 2017
European Planetary Science Congress 2017

Short-term variations of Mercury's cusps Na emission

S. Massetti[1], V. Mangano[1], A. Milillo[1], A. Mura[1], S. Orsini[1], and C. Plainaki[2]

(1) INAF-IAPS, Institute for Space Astrophysics and Planetology, Rome, Italy

(2) ASI, Italian Space Agency, Rome, Italy.

Abstract

We illustrate the analysis of short-term ground-based observations of the exospheric Na emission (D1 and D2 lines) from Mercury, which was characterized by two high-latitude peaks confined near the magnetospheric cusp footprints. During a series of scheduled observations from THEMIS solar telescope, achieved by scanning the whole planet, we implemented a series of extra measurements by recording the Na emission from a narrow north-south strip only, centered above the two emission peaks. Our aim was to inspect the existence of short-term variations, which were never analyzed before from ground-based observations, and their possible correlation with interplanetary magnetic field variations. Though Mercury possesses a miniature magnetosphere, characterized by fast reconnection events that develop on a timescale of few minutes, ground-based observations show that the exospheric Na emission pattern can be globally stable for a prolonged period (some days) and can exhibits fluctuations in the time range of tens of minutes.

Background

The study of Mercury's exosphere and its dynamics via ground-based observations of the bright sodium doublet emission (5890-96 Å) is an important way to understand the key processes lying behind the generation of the tenuous (collisionless) atmosphere of the small solar system bodies. The physical processes expected to play a role in the surface Na release are: strong bombardment by Solar Wind plasma driven by IMF-magnetosphere coupling, micrometeoroids impacts, Solar UV and thermal radiation, all weighted by the surface abundancies. Observations of the Na exosphere exhibit very often two high-latitude peaks usually symmetrically located in both hemispheres, along the subsolar meridian, but which also differ in intensity and/or extent. Their morphology and dynamics are conceivably associated to the direct precipitation of SW ions onto the surface (e.g. due to ion-sputtering & PSD processes), driven across the magnetospheric cusps by magnetic reconnection, since none of the other known release processes is able to produce such distinctive emission pattern by itself [1].

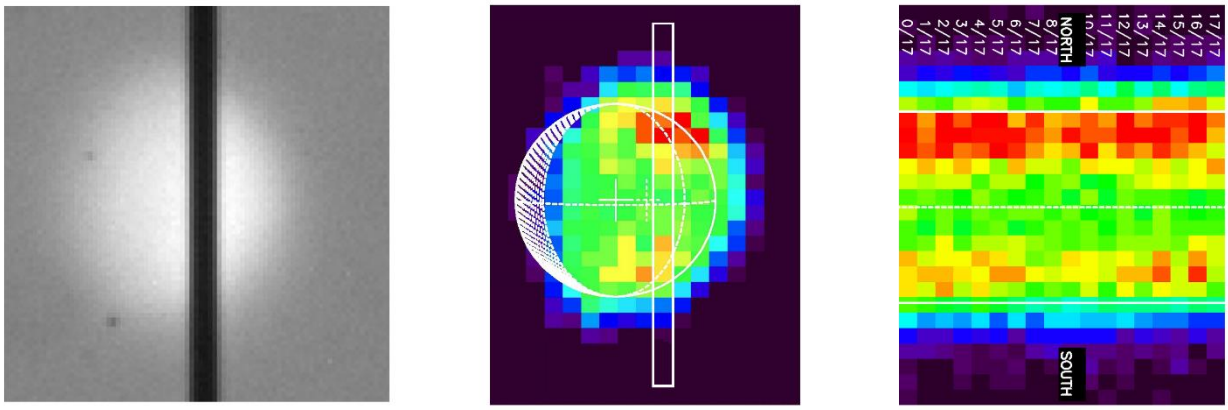

Figure – Sketch of the fixed-slit acquisition used by the authors to inspect short-term Na emission from the cusps. LEFT: spectrograph slit position over Mercury's disc (white light). CENTRE: slit position superimposed to a standard full disc Na image. RIGHT: time evolution of Na emission from 18 sequential North-South scans.

Data of the Na exosphere of Mercury are obtained by means of the THEMIS solar telescope (Tenerife, Canary Islands, Spain). THEMIS is equipped with a 0.9 m primary mirror with 15.04 m focal length that, thanks to its optical design, is characterized by a low level of scattered light. Because of this capability, it can be used during the daylight to image the Na exosphere of Mercury with a high contrast (with respect to sky brightness), for several hours per day.

Analysis and Conclusions

We inspect the time evolution of a steady double peaked Na exospheric emission at the Mercury's cusps that was observed to persist for more than three consecutive days (June 7-9, 2012). The southern Na emission was always narrower and weaker that the northern one, a fact which seems to conflict with the magnetic field model based on new data from Messenger [2], implying a wider southern cusp area. Given that the observed high-latitude Na emission is believed to be linked to the SW entry through the cusps, then a broader signal should be frequently observed from the southern hemisphere.

The lack of any significant one-to-one relationship between the observed Na exospheric emission intensity/morphology and the in-situ IMF data, matches the results of recent works that show that a low upstream Alfvénic Mach number - resulting in a low plasma β in the magnetosheath - can drive high reconnection rate at Mercury, nearly irrespective of the IMF direction [3][4].

A set of complementary fixed-slit observations show that the Na exospheric emission from both the North and the South hemispheres undergo a series of in-phase intensity oscillations on a timescale of 10-15 minutes. On the base of the available data is not possible to understand if these oscillations are real Na emission variations induced by SW perturbations, or just artifacts caused by atmospheric fluctuations (e.g.: changes in transparency).

Nevertheless, by means of a simple numerical model we show that such short-term variations, in the range 10-15 minutes, are compatible with the response time of the Na exospheric release, as induced by impulsive events (likely caused by ion precipitation).

Finally, by comparing the three fixed-slit images recorded on the first day (June 7), we detected a longer-term variation in the South/North emission ratio, on a timescale of about 1 hour, which definitely seems decoupled by local atmospheric fluctuations. This 1-hour variation is compatible with the Na photoionization lifetime and the fastest decay lifetime of simulated global Na exosphere, which takes place at small TAAs (≈ 0°- 60°), as in the present observations.

The results of this work have been recently published on Geophysical Research Letters [5].

Acknowledgements

Ground-based observation campaign of Mercury's Na exosphere from THEMIS was started and organized by F. Leblanc; the INAF participation is leaded by V. Mangano. Authors thanks the THEMIS staff in Tenerife (Canary Islands, Spain) for their fruitful help during the observation campaigns. This work was supported by the ASI-SERENA contract no. I/081/09/0 "SERENA: scientific activity". MESSENGER MAG data used in this study are available from the NASA Planetary Data System.

References

[1] Mangano et al. (2015), THEMIS Na exosphere observations of Mercury and their correlation with in-situ magnetic field measurements by MESSENGER. PSS, 115, 102-109, doi: 10.1016/j.pss.2015.04.001, 2015.

[2] Anderson et al. (2011), The Global Magnetic Field of Mercury from MESSENGER Orbital Observations, Science, 333, 1859-1862.

[3] DiBraccio et al. (2013), MESSENGER observations of magnetopause structure and dynamics at Mercury. J. Geophys. Res. Space Physics 118, 997-1008, doi:10.1002/jgra.50123.

[4] Slavin et al. (2014), MESSENGER observations of Mercury's dayside magnetosphere under extreme solar wind conditions, J. Geophys. Res. Space Physics, 119, 8087–8116, doi:10.1002/2014JA020319.

[5] Massetti et al. (2017), Short-term observations of double peaked Na emission from Mercury's exosphere. Geophys. Res Lett. 44, doi:10.1002/2017GL073090.

EPSC Abstracts
Vol. 11, EPSC2017-901, 2017
European Planetary Science Congress 2017

The BepiColombo/SERENA package: Serena Integrated Test campaign

Stefano Orsini (1), Elisabetta De Angelis (1), Stefano Livi (2), Herbert Lichtenegger (3), Stas Barabash (4), Anna Milillo (1), Peter Wurz (5), Angelo Olivieri (6), Luigi D'Arcio (7), Mark Phillips (2), Gunter Laky (3), Martin Wieser (4), Fabio Camozzi (8), Andrea M. Di Lellis (9), Rosanna Rispoli (1), Harald Jeszenszky (3), Alessandro Mura (1), Alessandro Aronica (1), Francesco Lazzarotto (1), Nello Vertolli (1), and Daniele Piazza (5).

(1)INAF-IAPS, Roma, Italy, (2)South-West Research Institute, San Antonio TX, USA, (3)Space Research Institute, Austrian Academy of Sciences, Graz, Austria, (4) Swedish Institute of Space Physics, Kiruna,Sweden, (5) Physics Institute, University of Bern, Switzerland, (6) Italian Space Agency, Roma, Italy, (7) ESA-ESTEC, Noordwijk, The Netherlands, (8) OHB-Italia SpA, Milano, (9) AMDL, Roma, Italy.

(stefano.orsini@iaps.inaf.it / Tel: +39 06 45488612)

Abstract

The activities related to the BepiColombo/ MPO/SERENA Integrated Test (SIT, held in February-March 2017 inside the thermal vacuum facility at the University of Bern, Phys. Inst.) are presented. This campaign has been a unique opportunity to test the experiment performances, with all the four flight-spare instruments of SERENA (ELENA, STROFIO, PICAM, and MIPA, simultaneously operated by the System Control Unit (SCU), in a fully operational configuration.

1. Introduction

The test is focused on the On-Board Commanding Procedure and on the Science Operation Basic Procedure, with the goal of providing a comprehensive picture of the on-board S/W facility both in nominal and more resource demanding conditions. Such a test is a powerful tool for allowing SERENA to perform the best possible observation of the particle populations surrounding Mercury.

2. SERENA package and SIT

SERENA (Search for Exospheric Refilling and Emitted Natural Abundances) [1] is an experiment on board the BepiColombo ESA/JAXA cornerstone mission to Mercury (to be launched in October 2018). It's the only particle instrument suite on board the Mercury Planetary Orbiter – MPO (400-1500 km). It addresses major scientific objectives of the BepiColombo mission, like solar-planet interaction processes and exospheric dynamics and composition. The interaction between energetic plasma particles, solar radiation and micrometeorites with the Hermean surface gives rise to both thermal and energetic neutral particle populations in the near-planet space; such populations will be recorded by the SERENA Neutral Particle Analysers (NPA): the neutral particle imager ELENA (Emitted Low Energetic Neutral Atoms) and the exosphere mass spectrometer Strofio (Start from a Rotating FIeld mass spectrometer).
The photo-ionised or charged component of the surface release processes as well as the precipitating and circulating plasma in the Hermean magnetosphere will be recorded by the SERENA ion spectrometers (IS): the planetary ion sensor PICAM (Planetary Ion CAMera) and precipitating ion sensor MIPA (Miniature Ion Precipitation Analyser). SERENA will provide information on the Hermean environment particle circulation and on the dynamical processes induced by the surface-exosphere-magnetosphere system when interacting with the solar wind and the interplanetary medium. Concerning these crucial aspects, joint measurements with similar instrumentation on board the Bepicolombo/MMO will allow to derive a comprehensive picture of the complex phenomena surrounding the planet.
The SIT is the first SERENA test performed with all the Flight Models in full functionality with real data. To perform full SERENA test is necessary to have all the units in high vacuum condition to switch on high voltage and detectors inside the instruments. A specific chamber with the requested conditions has been identified at Physic Institute in Bern. Ad-hoc configuration has been realized to have all the units

in vacuum condition (inside chamber) connected to the MIS and to the Instrument Ground Segment Equipment. The particular set-up (see Figure 1) for this important test was carried out with the support of several people of the SERENA team.

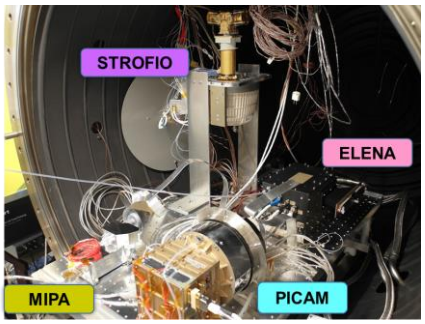

Figure 1: SERENA set-up inside the vacuum chamber.

The objectives of the SIT test are:
- to have all the 4 units running and generating real data (in vacuum condition);
- to verify OBCP command not performed during previous system tests (with HV on);
- to perform selected operation scenarios and investigate demanding cases in terms of telemetry, power and SCU resource constraints.

3. Summary and Conclusions

Thanks to this campaign all the units have been operated in science mode with real data. Several critical items have been pointed out and faced. An updated SERENA-SCU Flight software has been done and validated before the delivery to ESA. Thanks to the software update we demonstrate that the four units can be operated also in demanding configurations.

Acknowledgements

The research activities presented in this paper have been supported and funded by Italian Space Agency. The support of the University of Bern at the Phys. Institute has been fundamental for the success of this activity.

References

[1] Orsini, S., S. Livi, K. Torkar, S. Barabash, A. Milillo, P. Wurz, A. M. Di Lellis, E. Kallio and the SERENA team, "SERENA: a suite of four instruments (ELENA, STROFIO, PICAM and MIPA) on board BepiColombo-MPO for particle detection in the Hermean Environment", BepiColombo Special Issue on Planetary and Space Science, doi:10.1016/j.pss.2008.09.012, 58, 166-181, 2010

EPSC Abstracts
Vol. 11, EPSC2017-903-3, 2017
European Planetary Science Congress 2017

Spectral variations on H-2 Victoria quadrangle on Mercury: the case of Hokusai rays

F. Zambon (1), V. Galluzzi (1), C. Carli (1) F. Capaccioni (1), J. Wright (2), and D. A. Rothery (2)

(1) INAF-IAPS Istituto di Astrofisica e Planetologia Spaziali, Via del Fosso del Cavaliere, 100, I-00133 Rome, Italy;
(2) Open University, Walton Hall, Kents Hill, Milton Keynes MK7 6AA, UK. (francesca.zambon@iaps.inaf.it)

1. Introduction

Analysis of the Victoria quadrangle (H-2) on Mercury, performed by using multi-spectral mosaics from MESSENGER MDIS-WAC data, highlights a number of peculiar features (e.g. pyroclastic deposits, vents, smooth plains and crater ray systems). Here, we focus on the most widespread ray system on Mercury, the one related to the Hokusai impact crater (diameter = 96 km; 57.8°N, 16.8°E) [1, 2, 3, 4] (Figure 1), located in the namesake quadrangle (H-5) [5]. Hokusai ray system extends as far as 7000 km from the crater center, and is distributed about the cavity with the largest concentration of rays located toward the southwest [1]. On Mercury's surface, several other crater ray systems other than Hokusai have been detected (e.g. Debussy, Degas and Kuiper). Furthermore, similar ray systems have also been observed on other bodies of the Solar System, such as the Moon, Mars and the icy satellites, in particular Ganymede [6]. Tens of craters with ray system have been observed on the Moon, while Mars and Mercury have a comparable number. Unlike Ganymede, on Mercury, no correlation between longitude and ray crater distribution has been observed, although the longest rays are located around 0° longitude [6]. The presence of rays indicates that Hokusai is a young crater, formed during the Kuiperian system. This system extends from the present day to 100-300 Myr [1], placing an upper limit on Hokusai's age. The ratio of ray length to crater diameter for Hokusai's ten longest rays is approximately 55 to 1, a value that is anomalously high compared even with the outliers in previous measurements [7, 8, 1]. Here, we investigate Hokusai ray composition by considering multispectral data from the MDIS-wide angle camera onboard MESSENGER.

2. Dataset description

The Mercury Dual Imaging System (MDIS) [9], mapped the Hermean surface at different spatial resolutions, due to the variable spacecraft altitude. MDIS consists of two instruments: a Narrow Angle Camera (NAC) centered at ~747 nm, which acquired high-resolution images for the geological analysis, and the Wide Angle Camera (WAC), provided with 11 filters dedicated to the compositional analysis, operating in a range of wavelengths between ~395 and ~1040 nm [9]. We produced a color mosaic by using the images relative to the filters with the best spatial coverage. To obtain the 8-color mosaic of the region of interest, we calibrated and georeferenced the WAC raw images. Afterwards, we applied the Hapke photometric correction by using the parameters derived by [10]. We projected and coregistered the data, and finally, we produced the mosaic. Subsequently, we consider different techniques of analysis, such as band ratio, RGB color combination and classification methods, to derive the spectral behavior of Hokusai ray system.

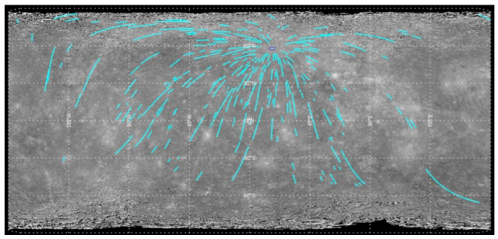

Figure 1: Hokusai crater ray map shown in [1], which displays their distribution over a large part of Mercury's surface

3. Results

The spectral analysis of Victoria quadrangle, highlights spectral variations mostly in correspondence of the Hokusai rays. Applying different techniques of analysis, such as band ratio

(Figure 2) and classification methods to selected spectral ratios (628nm/433nm, 828nm/628nm, 996nm/828nm, 996nm/433nm), we can identify region with different spectral characteristics. Fist results obtained by using K-mean [11] clustering method allow for identifying three classes: one for Hokusai rays, one for the intercrater plains [12], widespread within the quadrangle and one for the smooth plains in the north-western part of H-2. Since Mercury spectra are mainly characterized by spectral slope variations, our results allow for defining areas with different behaviour in terms of this specific spectral parameter. The spectral slope is a useful parameter to investigate surface properties, being associated, for example, with terrain's maturity and variation in particle size or terrain's roughness [13, 14]. Lower spectral slope can be associated with young terrains, while higher spectral slope values are typical of older terrains (e.g. [14]). Here, we found that Hokusai rays belong to the class characterized by lower spectral slope, according with the younger age of this structure. The smooth plain region has higher spectra slope, while the intercrater plains areas present intermediate values. In future work, we will continue the analysis of the Hokusai ray system also outside Victoria quadrangle, comparing it with other similar features both on Mercury and on other bodies of the Solar System. The identification and the study of regions of interest on Mercury is useful to define possible targets for the SIMBIO-SYS instrument onboard the future BepiColombo mission.

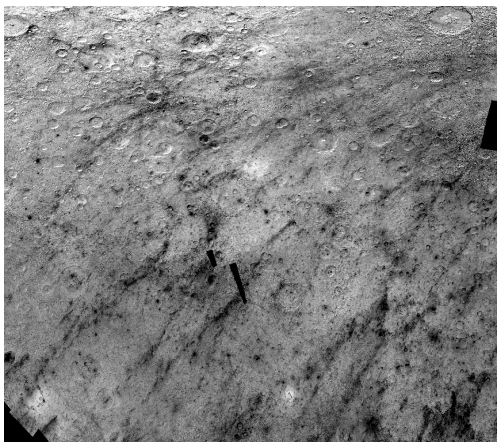

Figure 2: Portion of the Victoria quadrangle that encompasses Hokusai rays. The image obtained by MDIS-WAC data displaying the ratio between the filters at 996 nm and 558 nm. This ratio emphasizes Hokusai rays, which appear darker than the rest of the quadrangle, indicating lower reflectance at longer wavelengths.

Acknowledgements

This work was supported by the Italian Space Agency (ASI) within the SIMBIO-SYS project (ASI-INAF contract no. I/022/10/0).

References

[1] C. M. Ernst et al., 47th LPSC, abstract #1374, 2016.

[2] Harmon, J.K. et al. (2007) *Icarus*, *187*, 374–405.

[3] Z. Xiao et al., Bridging the Gap III, abstract #1064, 2015.

[4] Z. Xiao et al., Geophys. Res. Lett., 43, 7424-7432, doi:10.1002/2016GL069868, 2016

[5] D. A. Rothery et al., 48th LPSC, abstract #1406, 2017

[6] J. Szczeszek et al., 47th LPSC, abstract #3024, 2016.

[7] Gault, D.E. and Wedekind, J.A. *Proc. Lunar Planet. Sci. Conf., 9,* 3843–3875, 1978

[8] Herrick, R.R. and Forsberg Taylor, N.K. *Meteorit. Planet. Sci., 38*, 1551–1578, 2003.

[9] S. E. Hawkins III et al., pp 247-338. Doi: 10.1007/978-0-387-77214-1_9, Springer, 2007-

[10] D. Domingue et al., Icarus 257 (2015) 477–488. Doi: http://dx.doi.org/10.1016/j.icarus.2014.11.027, 2015.

[11] J. B. MacQueen, Proceedings of 5-th Berkeley Symposium on Mathematical Statistics and Probability, Berkeley, University of California Press, 1:281-297, 1967

[12] V. Galluzzi et al., Journal of Maps, 2016.

[13] R. Clark, John Wiley and Sons, Inc A. Rencz, Editor New York, 1999

[14] K. Stephan et al., An investigation of the bluish material on Ceres.GRL 44, 1660–1668, 2017.

EPSC Abstracts
Vol. 11, EPSC2017-976, 2017
European Planetary Science Congress 2017

The Intermediate Plains of Mercury: considerations on a debated unit

V. Galluzzi (1), C. Carli (1), F. Zambon (1), L. Giacomini (1), L. Guzzetta (1), L. Ferranti (2) and P. Palumbo (3,1)
(1) INAF, Istituto di Astrofisica e Planetologia spaziali (IAPS), Rome, Italy (valentina.galluzzi@iaps.inaf.it); (2) DiSTAR, Dipartimento di Scienze della Terra, dell'Ambiente e delle Risorse, Università "Federico II", Naples, Italy; (3) Dipartimento di Scienze & Tecnologie, Università degli Studi di Napoli 'Parthenope', Naples, Italy.

Abstract

The ongoing production of a 1:3M-scale geological map of Mercury has permitted a deepened study of a debated terrain unit: the Intermediate Plains. It was introduced during the past Mariner 10 1:5M-scale geological mapping campaign, and lately it has been discarded and encompassed into either the Smooth Plains unit or the Intercrater Plains unit by the MESSENGER team. However, our studies show that for some limited areas, this unit has a distinct age, morphology, evolution and possibly composition.

1. Introduction

On Mercury 'surface morphology reflects the age, composition, lithology, and mode of formation of the underlying rock unit' [1] and Mercury's *geological provinces* must be 'characterized by a similar inferred origin or a distinctive history' [2, 3]. Based on these statements, three main morphologically recognizable units historically characterize the surface of Mercury: Smooth Plains (SP), Intercrater Plains (ICP) and Intermediate Plains (IMP). The latter, form 'planar to undulating surfaces that have higher crater density than smooth plains material, but are less heavily cratered than intercrater plains material' [4]. However, recent works conclude that there is no clear contrast between IMP and the adjacent terrains, such that they can be encompassed into either SP or ICP units [5], and that the age of IMP and ICP seem to overlap [6]. For these reasons, the IMP unit has been lately discarded from some geological maps [5, 7]. The recent production of a series of 1:3M-scale geological maps [e.g. 8, 9], however, led to the re-introduction of this unit due to evident morphological peculiarities that are visible at the used mapping scale (~1:400k). This is particularly clear in the area encompassed between the Holbein, Geddes and Vlaminck craters mapped by [8], where a distinct crater density and different structures characterize an IMP terrain patch (Fig. 1). The probable distinct evolution of this area of Mercury is also corroborated by a peculiar composition when compared to the geochemical terrains detected by [10]. With this work we look forward to better characterizing the mapped IMP regions by means of photo-interpretation, relative and absolute age determination, spectral and colour analysis, and correlation with element ratio composition in order to understand which events determined their evolution.

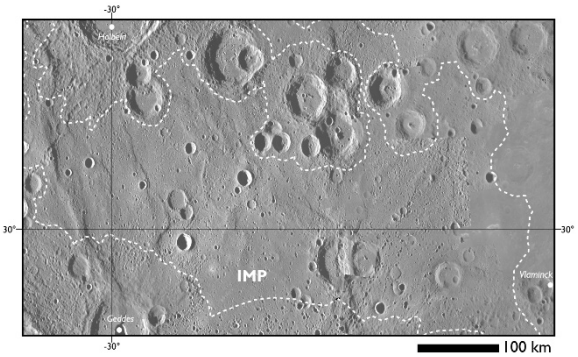

Figure 1: The Intermediate Plains of Mercury in the area encompassed between Holbein, Geddes and Holbein craters (inside the dashed line, marked with IMP). Unit boundaries mapped by [8]. Equirectangular projection.

2. Data and methods

We mainly use the data collected by the Mercury Dual Imaging System (MDIS) on-board the MErcury Surface, Space Environment, Geochemistry and Ranging (MESSENGER) mission. We selected some photo-interpreted IMP areas from the map of [8] and made a thorough analysis of their morphology and features. We estimated the relative and absolute age of IMP and its overlapping features by means of crater counting techniques. We aim at correlating these results to the updated chemical information derived by the MESSENGER X-Ray Spectrometer (XRS) [11] and the available MDIS colour basemaps (MDR, MD3) or self-produced higher-resolution colour mosaics [12].

3. Results and future work

Current results show that the analysed IMP areas (Fig. 2) have an average crater frequency of 80±17 (normalized to an area of 10^6 km^2) for craters larger than 20 km, while SP and ICP crater frequencies are 40±10 and 114±13, respectively. Their absolute age results to be ~3.9±0.1 Ga, almost overlapping with the age of ICP, which is ~4.0±0.1 Ga in the studied area. Thus, they seem to remain a distinct unit both for their morphology and for their age. However, they pertain to two different geochemical terrains detected by [10]. One is characterized by high-Al abundance that stands out with respect to the adjacent plains and approximately corresponds to an area previously mapped as SP by [5]; the other, is encompassed in the high-Mg region, denoting a probable different origin. This compositional variability should reflect a different rock-forming mineralogy, which could be evidenced also by spectral variability in MDIS data.

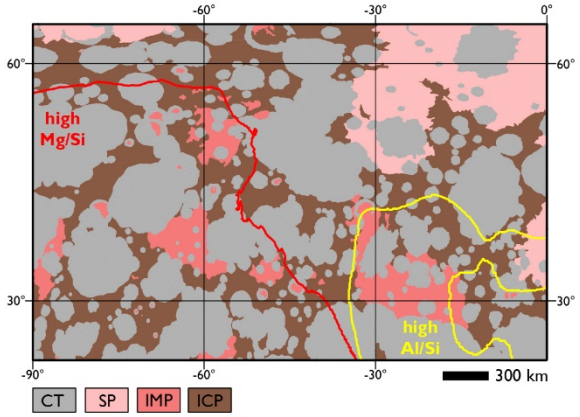

Figure 2: Simplified geological scheme of the Victoria quadrangle derived from the geological map of [8] showing the contour lines of the High-Mg region (Mg/Si > 0.5 in red) and of the high-Al region (Al/Si > 0.3 in yellow) [11]. Equirectangular projection centered at lat. 43.75°N, lon. -45°E. CT=Cratered Terrain, SP=Smooth Plains, IMP=Intermediate Plains, ICP=Intercrater Plains.

Finally, this evidence might lead to detect two distinct sub-units to obtain local- to regional-scale advanced geological maps that will rely on both surface morphology and mineralogy. In this view, our observations lead to the retention of Intermediate Plains as an official unit of Mercury, but further work is needed in order to contextualize their controversial nature.

Acknowledgements

This research was supported by the Agenzia Spaziale Italiana (ASI) within the SIMBIOSYS project (ASI-INAF agreement n. I/022/10/0).

References

[1] Trask, N. J. & Guest, J. E., Journal of Geophysical Research, 80, 2461–2477, 1975.

[2] Spudis, P. D. & Guest, J. E., In: Vilas, F., et al. (eds), Mercury, 118–164, University of Arizona Press, 1988.

[3] McCauley, J. F. & Wilhelms, D. E., Icarus, 15, 363–367, 1971.

[4] Spudis, P. D. & Prosser, J. G., US Geological Survey, Map I-1659, 1984.

[5] Denevi, B. W. et al., Journal of Geophysical Research: Planets, 118 (5), 891–907, 2013.

[6] Whitten, J. L. et al., Icarus, 241, 97–113, 2014.

[7] Prockter, L. M. et al., Lunar and Planetary Science Conference, 47th, #1245, 2016.

[8] Galluzzi, V. et al., Journal of Maps, 12, 227–238, 2016.

[9] Guzzetta, L. et al., Journal of Maps, 13, 227–238, 2017.

[10] Weider, S. Z. et al., Earth and Planetary Science Letters, 416, 109–120, 2015.

[11] Nittler, L. R. et al., Lunar and Planetary Science Conference, 47th, #1237, 2016.

[12] Zambon, F. et al., Geophysical Research Abstracts,19, EGU2017-16900, 2017.

EPSC Abstracts
Vol. 11, EPSC2017-1005, 2017
European Planetary Science Congress 2017

Building up the 1:3M geological map of Mercury

V. Galluzzi (1), L. Guzzetta (1), P. Mancinelli (2), L. Giacomini (1), C. Malliband (3), A. Mosca (4), J. Wright (3), L. Ferranti (4), M. Massironi (5), C. Pauselli (2), D. A. Rothery (3), and P. Palumbo (6,1)
(1) INAF, Istituto di Astrofisica e Planetologia spaziali (IAPS), Rome, Italy (valentina.galluzzi@iaps.inaf.it); (2) Dipartimento di Fisica e Geologia, Università degli Studi di Perugia, Perugia, Italy; (3) School of Physical Sciences, The Open University, Milton Keynes, UK; (4) DiSTAR, Dipartimento di Scienze della Terra, dell'Ambiente e delle Risorse, Università "Federico II", Naples, Italy; (5) Dipartimento di Geoscienze, Università degli Studi di Padova, Padua, Italy; (6) Dipartimento di Scienze & Tecnologie, Università degli Studi di Napoli 'Parthenope', Naples, Italy.

Abstract

The 1:3M-scale geological map series of Mercury was born from individual quadrangle mapping products and has proceeded toward a global mapping project that will be released as a digital global output. The MESSENGER data and reference systems used for this project underwent several changes over the past years. Here we report how we dealt with these updates and the status of our work.

1. Introduction

By the end of the NASA Mariner 10 mission (1973-1979), 45% of Mercury's surface had been imaged by the M10 Television Experiment and over 2000 useful pictures were available at a resolution better than 2 km, up to 100 m. These results led to the production of 1:5M geologic maps of seven of the fifteen quadrangles of Mercury [1]. The NASA MESSENGER (MErcury Surface, Space ENvironment, GEochemistry and Ranging; 2004-2015) mission filled the gap by imaging 100% of the planet with a frame resolution up to 8 m/pixel at the north pole, and a global average resolution of 200 m/pixel, enabling preparation of a new global 1:15M geologic map [2]. Today, a complete global series of 1:3M-scale global maps of Mercury is being prepared in support to the BepiColombo joint mission of the European Space Agency (ESA) and the Japan Aerospace Agency (JAXA) [3]. Born from individual geologic quadrangle maps [4, 5, 6], it has evolved into a coordinated global mapping plan, and carried on with the aim of exploiting MESSENGER images at the best resolution available (i.e., global average resolution) in order to set up the context for BepiColombo operations and help re-define mission goals as appropriate. In the early part of the project, the data coming from the still ongoing MESSENGER mission were constantly changed and updated. This required a careful check of our products, and eventually will require a transformation of the linework in the light of the newly released MESSENGER end-of-mission datasets.

2. Available Datasets

2.1. Past datasets

When this project started, the MESSENGER mission was still releasing datasets, and this caused basemap coverage and resolution to change frequently. Since most basemaps were initially released as 250 m/pixel mosaics, the best dataset that could be used as a reference basemap was the 166 m/pixel map-projected Basemap reduce Data Record (BDR). These resolutions permit us mapping at scales of ~1:300,000 to ~1:600,000. The Mercury Laser Altimeter (MLA) provided also a 500 m grid Digital Elevation Model (DEM) for the North Pole and a 665 m grid DEM for the Northern hemisphere [7]. This was the main reason why the mapping project started from the Northern hemisphere.

2.2. End-of-Mission Datasets

By the end of the MESSENGER mission several new global basemaps at 166 m/pixel were released: a new BDR, two high incidence angle basemaps with illumination from East and West (HIE and HIW), and a low incidence angle basemap (LOI). Moreover, the United States Geological Survey (USGS) has made available a 665 m global coverage DEM derived from stereo-imaging [8], providing a better understanding also of the Southern hemisphere.

2.3. Reference system issues

The MESSENGER team approximated Mercury's radius to 2440.0 km during the operational phase of the mission, thus our first map products followed the same datum. With the end-of-mission datasets release, this datum was updated to 2439.4 km. Moreover, the prime meridian definition slightly changed, causing a latitudinal shift of the basemaps of almost 0.1°

westward. This shift is not constant however, since the new basemaps are now controlled and projected onto the new USGS DEM. Since we are going to use the end-of-mission basemaps for the new products, the already produced maps will require a careful transformation in order to avoid a mismatch. The transformation will take into account the new sphere radius, the new prime meridian shift, and possibly, the USGS shape-model.

3. Current results

Currently, H02 Victoria [4], H03 Shakespeare [6] and H04 Raditladi [5] have been completed; H05 Hokusai [9], H06 Kuiper [10], H07 Beethoven and H10 Derain [11] are being mapped (Fig. 1). The produced geologic maps were merged adjusting mismatches along the quadrangle boundaries. Contact discrepancies were reviewed and discussed among the mappers of adjoining quadrangles in order to match the geological interpretation and provide a unique consistent stratigraphy.

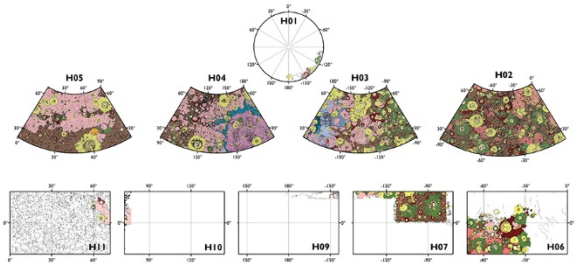

Figure 1: Current status of the 1:3M-scale geological map series of Mercury for the Northern hemisphere quadrangles. The used projections are centered on each quadrangle: H01 Polar Stereographic; H02 to H05 Lambert Conformal Conic with standard parallels at 30°N and 58°N; H06 to H10 Equidistant Cylindrical.

At the current stage, about 30% of Mercury has now a complete 1:3M-scale map and more than 40% of the planet will be covered soon by the maps that are being prepared. This series of 1:3M-scale quadrangle maps cannot be merged into a single physical 1:3M-scale global map. However, the global merged output will be used as a digital full-scale product, which will permit detailed global or regional analyses of Mercury's surface. This project will lead to a fuller grasp of the planet's stratigraphy and surface history and is an important goal in preparation for the forthcoming ESA/JAXA BepiColombo mission to aid selection of scientific targets and to provide context for interpretation of new data.

Acknowledgements

This research was supported by the Agenzia Spaziale Italiana (ASI) within the SIMBIOSYS project (ASI-INAF agreement n. I/022/10/0).

References

[1] Spudis, P. D. & Guest, J. E., In: Vilas, F., et al. (eds), Mercury, 118–164, University of Arizona Press, 1988.

[2] Prockter L. M., et al., XLVII LPSC, Abs. #1245, 2016.

[3] Benkhoff, J. et al., Planetary and Space Science, 58, 2–20, 2010.

[4] Galluzzi, V. et al., Journal of Maps, 12, 227–238, 2016.

[5] Mancinelli, P. et al., Journal of Maps, 12, 190–202, 2016.

[6] Guzzetta, L. et al., Journal of Maps, 13, 227–238, 2017.

[7] Zuber, M. T. et al., Science, 336, 217–2202011.

[8] Becker, K. J. et al., XLVII LPSC, Abs. #2959, 2016.

[9] Rothery, D. A. et al., XLVIII LPSC, Abs. #1406, 2017.

[10] Giacomini, L. et al., Geophysical Research Abstracts, 19, EGU2017-14574-1, 2017.

[11] Malliband, C. C. et al., XLVIII LPSC Abs., #1476, 2017.

EPSC Abstracts
Vol. 11, EPSC2017-1006-1, 2017
European Planetary Science Congress 2017

Geology of the Shakespeare quadrangle (H03), Mercury

L. Guzzetta (1), V. Galluzzi (1), L. Ferranti (2) and P. Palumbo (3,1)
(1) INAF, Istituto di Astrofisica e Planetologia spaziali (IAPS), Rome, Italy (laura.guzzetta@iaps.inaf.it); (2)DiSTAR, Dipartimento di Scienze della Terra, dell'Ambiente e delle Risorse, Università "Federico II", Naples, Italy; (3) Dipartimento di Scienze & Tecnologie, Università degli Studi di Napoli "Parthenope", Naples, Italy.

Abstract

A 1:3M geological map of the H03 Shakespeare quadrangle of Mercury has been compiled through photointerpretation of the remotely sensed images of the NASA MESSENGER mission. This quadrangle is characterized by the occurrence of three main types of plains materials and four basin materials, pertaining to the Caloris basin, the largest impact crater on Mercury's surface. The geologic boundaries have been redefined compared to the previous 1:5M map of the quadrangle and the craters have been classified privileging their stratigraphic order rather than morphological appearance. The abundant tectonic landforms have been interpreted and mapped as thrusts or wrinkle ridges.

1. Introduction

The observations of Mercury's surface made by the Mariner 10 (M10) and MESSENGER spacecraft have shown that Mercury displays a moderately cratered surface, several plains deposits and abundant lunar-type landforms which were interpreted as superficial expression of compressive tectonic structures [1]. With the first 1:5M geological maps of some quadrangles, based on M10 data, craters were mapped according to their degree of degradation and grouped into five classes from the oldest c1 to the youngest c5 [5]. The plains deposits were distinguished according to their morphologies and textures in smooth, intermediate and intercrater plains materials [3], [7]. In the H03 quadrangle were also distinguished peculiar morphologies associated with the Caloris basin [5]. Notwithstanding the MESSENGER images have a better global average resolution with respect to those of M10, only a global 1:15M geological map has been produced [6]. The most evident novelty of the geological map here presented is the adoption of a different crater classification, which solves some stratigraphic inconsistences derived from the five-class classification system when dealing with small craters. A better correlation between morphology and geological boundaries led to a significant redefinition of the spatial distribution of the intercrater and intermediate plain materials.

2. Data and methods

Mapping was performed on a reference monochromatic basemap of reflectance at 166 m/pixel resolution of the H03 quadrangle, located at middle-latitude of the northern hemisphere of Mercury. A suite of a lower resolution basemaps, useful for their different lighting conditions, and two available DTM's, useful in sectors with non-optimal lighting geometry, were also consulted. The datum adopted is that used in the data sets released by the MESSENGER team, in which Mercury's IAU radius (2439.7 km) is approximated to 2440.0 km. The most suitable projection at middle-latitudes is the Lambert conformal conic, as it reduces area distortions. The geological features were digitized within a geographic information system with a variable mapping scale between 1:300k and 1:600k. Craters were distinguished into those with $10 \leq D < 20$ km (small), for which only rim crests were mapped, and craters with $D \geq 20$ km (major), for which also crater materials were mapped and grouped into three morpho-stratigraphic classes (c1-c3) according to their overlapping relationships [2]. Based on the dominant contractional nature of Mercury's tectonics [1], [8], the structures have been interpreted as thrusts, if they show a relevant break in slope and a sinuous trace, or as wrinkle ridges, which generally show a less prominent ridge and occur within smooth plain materials and basins. The geologic contacts were mapped as 'certain' where they are clear and sharp, or 'approximate' where they are uncertain or gradational. The geologic units were distinguished according to their morphological aspects and following definitions of previous authors [3]. Other geomorphological elements such as 'hollows', crater chains and clusters, light coloured ejecta and bright deposits have also been mapped when their width is ≥ 3 km.

3. Map description

The intercrater plain (ICP) and smooth plain (SP) materials are the main plain materials of the quadrangle occurring in the eastern and west-central sector, respectively. The intermediate plain (IMP) materials occur only as small patches, mostly in the eastern area of the map. The basin materials, mapped in the western sector of the quadrangle, are associated with the Caloris basin and have been distinguished according to four formations (Caloris Group) termed with official names [5]. Tectonic structures mainly occur in this sector of the quadrangle. They have been gathered according to two preferential orientations: in the NE of Caloris, NE–SW trending thrusts appear to form a radial pattern with respect to the basin geometry, whereas the wrinkle ridges are mainly oriented between N10°E and N15°E. To the E of the basin, the NNE–SSW oriented thrusts and wrinkle ridges appear to have a non-radial geometry with respect to Caloris (Figure 1).

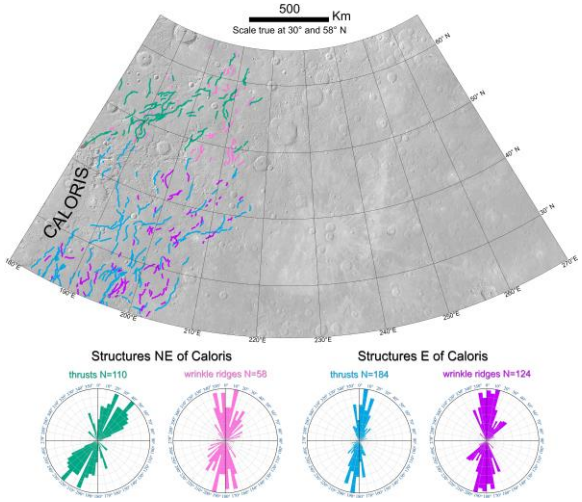

Figure 1: Distribution of the mapped structures nearby the Caloris basin and relative azimuth-frequency diagrams showing the main trend for thrusts and wrinkle ridges, respectively.

4. Summary and Conclusions

The MESSENGER images have allowed production of a more detailed 1:3M cartographic product of the Shakespeare quadrangle with respect to the previous 1:5M map. The craters were distinguished according to their diameter size in 'small' and 'major' craters. By integrating morphology, size and stratigraphy, the 'major' craters were grouped into three degradation classes, which allowed us to reduce the error in assigning relative ages. The western sector of the quadrangle is occupied by a portion of the Caloris basin and associated ejecta, which are embayed and partly covered by smooth plains deposits. The detected morpho-structures have contributed to an assessment of the deformation pattern of the quadrangle and will contribute to better evaluation of past stress states of the planet. This geologic map fills the gap between the two 1:3M maps of the Raditladi [4] and Victoria [2] quadrangles and can be considered an important support to future advanced local studies and target selection for the scheduled ESA-JAXA BepiColombo mission to Mercury.

Acknowledgements

The authors acknowledge the use of MESSENGER data processed by NASA/Johns Hopkins University Applied Physics Laboratory/Carnegie Institution of Washington. This research was supported by the Agenzia Spaziale Italiana (ASI) within the SIMBIOSYS project (ASI-INAF agreement n. I/022/10/0).

References

[1] Byrne, P. K., Klimczak, C., Şengör, A. C., Solomon, S. C., Watters, T. R., and Hauck, II, S. A.: Mercury's global contraction much greater than earlier estimates. Nature Geoscience, Vol 7(4), pp. 301–307, 2014.

[2] Galluzzi, V., Guzzetta, L., Ferranti, L., Di Achille, G., Rothery D. A., and Palumbo, P.: Geology of the Victoria Quadrangle (H02), Mercury. Journal of Maps, 2016.

[3] Guest, J. E. and Greeley, R.: Geologic map of the Shakespeare quadrangle of Mercury. Miscellaneous Investiagtions Series USGS, Map I-1408, 1983.

[4] Mancinelli, P., Minelli, F., Pauselli, C., and Costanzo, F.: Geology of the Raditladi quadrangle, Mercury (H04). Journal of Maps, 2016.

[5] McCauley, J. F., Guest, J. E., Schaber, G. G., Trask, N. J. and Greeley, R.: Stratigraphy of the Caloris basin, Mercury. Icarus, Vol 47(2), pp. 184–202, 1981.

[6] Prockter L. M., Kinczyk, M. J., Byrne, P. K., et al.,: The First Global Geological Map of Mercury. 47th LPSC, 21-25 March 2016, The Woodlands, Texas, 2016.

[7] Spudis, P. D., and Guest, J. E.: Stratigraphy and geologic history of Mercury. In F. Vilas, C. R. Chapman, & M. S. Matthews (Eds.), Mercury, pp. 118–164, University of Arizona Press, 1988.

[8] Watters, T. R. and Nimmo, F.: The tectonics of Mercury, in T. R. Watters and R. A. Schultz (Eds.), Planetary tectonics, pp. 15–80. Cambridge University Press, 2010.